



1 **Overdeepening or tunnel valley of the Aare glacier on the northern margin of the European**
2 **Alps: Basins, riegels, and slot canyons**

3
4 Fritz Schlunegger¹, Edi Kissling², Dimitry Bandou^{1,3}, Guilhem Douillet¹, David Mair¹, Urs Marti⁴,
5 Regina Reber¹, Patrick Schläfli^{1,5}, and Michael Schwenk^{1,6}

6
7 ¹Institute of Geological Sciences, University of Bern, Baltzerstrasse 1+3, 3012 Bern, Switzerland

8 ²Department of Earth Sciences, ETH Zürich, Sonneggstrasse 5, 8092 Zürich, Switzerland

9 ³Department of Environmental Sciences, University of Virginia, 291 McCormick Rd., Charlottesville,
10 VA 22904-4123, USA

11 ⁴Landesgeologie Swisstopo, Seftigenstrasse 264, Postfach, 3084 Wabern, Switzerland

12 ⁵Institute of Plant Sciences and Oeschger Centre for Climate Change Research, Altenbergrain 21,
13 3013 Bern, Switzerland

14 ⁶Bayerisches Landesamt für Umwelt, Umweltdienstleistungen, Hof, 95030 Hof Saale, Germany

15

16 fritz.schlunegger@unibe.ch

17

18 **Abstract**

19 This work summarizes the results of an interdisciplinary project where we aimed to explore the origin
20 of overdeepenings or tunnel valleys through a combination of a gravimetry survey, drillings, dating and
21 a synthesis of previously published work. To this end, we focused on the Bern area, Switzerland,
22 situated on the northern margin of the European Alps. In this region, multiple advances of piedmont
23 glaciers during the Quaternary glaciations resulted in the carving of the main overdeepening of the Aare
24 River valley (referred to as Aare main overdeepening). This bedrock depression is tens of km long and
25 up to several hundreds of meters to a few kilometers wide. We found that in the Bern area, this main
26 overdeepening is made up of two >200 m-deep troughs that are separated by a c. 5 km-long and up to
27 150 m-high transverse rocky ridge, interpreted as a riegel. The basins and the riegel are overlain by a
28 >200 m- and 100 m-thick succession of Quaternary sediments, respectively. The bedrock itself is made
29 up of a Late Oligocene to Early Miocene suite of consolidated clastic deposits, which are part of the
30 Molasse foreland basin, whereas the Quaternary suite comprises a middle Pleistocene to Holocene
31 succession of glacio-lacustrine gravel, sand and mud. A synthesis of published gravimetry data revealed
32 that the upstream stoss side of the bedrock riegel is c. 50% flatter than the downstream lee side. In
33 addition, information from >100 deep drillings reaching depths >50 m suggests that the bedrock riegel
34 is dissected by an anastomosing network of slot canyons. We propose that these canyons established
35 the hydrological connection between the upstream and downstream basins during their formation.
36 Based on published modelling results, we interpret that the riegels and canyons were formed through



37 incision of subglacial meltwater during a glacier's decay state, when large volumes of meltwater were
38 released. Such a situation has repeatedly occurred since the Middle Pleistocene Transition
39 approximately 800 ka ago, when large and erosive piedmont glaciers began to advance far into the
40 foreland. This resulted in the deep carving of the inner-Alpine valleys, and additionally in the formation
41 of overdeepenings on the plateau on the northern margin of the Alps.

42

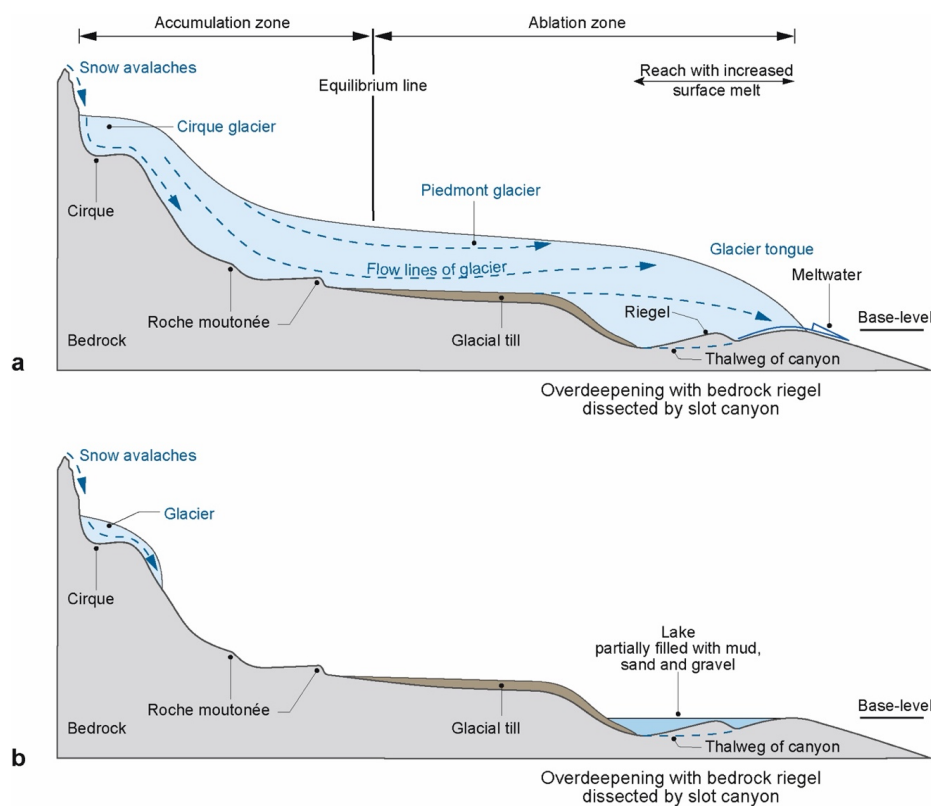
43 **1 Introduction**

44 Overdeepenings, or tunnel valleys (e.g., Jørgensen and Sandersen, 2006; Dürst Stucki et al., 2010), are
45 bedrock depressions below the current fluvial base-level (Fischer and Häberli, 2012). The downstream
46 closures of these basins have adverse slopes that generally dip in the upstream direction (Häberli et al.,
47 2016). Because bedrock depressions with such characteristics are commonly found in previously
48 glaciated areas (Figure 1), their formation has been interpreted as resulting from the erosional work of
49 glaciers with support by subglacial meltwater (Wright, 1973; Herman and Braun, 2008; Egholm et al.,
50 2009; Kehew et al., 2012; Patton et al., 2016; Liebl et al., 2023; and many others). Overdeepenings have
51 been reported for the Quaternary from beneath the Greenland and Antarctic glaciers (Ross et al., 2011;
52 Patton et al., 2016), the North Sea (Moreau et al., 2012, Lohrberg et al., 2022), North America (Wright,
53 1973; Lloyd et al., 2023) and northern Europe including Scandinavia (Clark and Walder, 1994;
54 Piotrowski, 1997; Kron et al., 2009). In addition, numerous Paleozoic successions entailing glaciogenic
55 paleovalleys were also described (e.g. Douillet et al., 2012; Dietrich et al., 2021). Such erosional troughs
56 have particularly been identified in the European Alps (Preusser et al., 2010), where >200 m-deep and
57 several km-long bedrock depressions beneath the modern base-level occur in the Alpine valleys as well
58 as on foreland plateaus on either side of this mountain belt (Preusser et al., 2010; Dürst Stucki and
59 Schlunegger, 2013; Magrani et al., 2020). Geophysical surveys (e.g., Rosselli and Raymond, 2003;
60 Reitner et al., 2010; Stewart and Lonergan, 2011; Stewart et al., 2013; Perrouy et al., 2015; Burschil et
61 al., 2018; 2019; Ottesen et al., 2020) in combination with drillings (Jordan, 2010; Dürst Stucki et al.,
62 2010; Büchi et al., 2017; 2018; Gegg et al., 2021; Bandou et al., 2022; 2023; Anselmetti et al., 2022;
63 Schwenk et al., 2022a, b; Gegg and Preusser, 2023; Schaller et al., 2023) disclosed that such
64 overdeepenings can be several kilometers wide and tens of kilometers long and that they are generally
65 made up of individual sub-basins separated by bedrock swells, or riegels (Cook and Swift, 2012).
66 Bedrock swells or riegels that separate bedrock depressions have also been reported from modern
67 landscapes. In this context, a riegel is a rock wall, which is oriented across a previous glacier's flow
68 direction.

69 An ensemble consisting of a riegel separating upstream and downstream basins has been considered as
70 a classical feature of a landscape, which was repeatedly sculpted by glaciers during the past glaciations
71 (Brocklehurst and Whipple, 2002; Brocklehurst et al., 2008; Cook and Swift, 2012; Steinemann et al.,
72 2021). Observations from modern landscapes (see Figure 2 for examples in the Swiss Alps) have



73 additionally shown that such bedrock swells or riegels may be cut by slot canyons or inner gorges
 74 (Montgomery and Korup, 2011; Steinemann et al., 2021), establishing a hydrological link between the
 75 upstream and downstream basins. These features were used as key information for invoking dissection
 76 by meltwater as an important erosional mechanism (Carter and Anderson, 2006; Steinemann et al.,
 77 2021). Although bedrock swells or riegels were reported as common features in overdeepenings (Gegg
 78 and Preusser, 2023), the occurrence of inner gorges or slot canyons (Figure 1) have only recently been
 79 disclosed (Bandou et al., 2023). It is the scope of this work to document such structures in an
 80 overdeepening and to discuss their importance for our understanding of how such depressions were
 81 formed.



82

Figure 1

Figure 1: Architecture of a landscape sculpted by piedmont glaciers during glaciations. a) Situation immediately following a full glacial period during which a piedmont glacier, which extended far into the foreland, started to melt. As a result, large volumes of meltwater are produced in the ablation zone close to the glacier's tongue. This meltwater has the potential to contribute to the erosional downwearing of the bedrock, and it can cause the incision of canyons into bedrock riegels, which separate two overdeepened basins. b) During interglacial time periods, the piedmont glaciers disappear, and small ice caps may be preserved in the higher parts of a mountain belt. During this time, the overdeepened basin will be filled by lacustrine sediments and will eventually host a lake. Modified after Schlunegger and Garefalakis (2023).

83



84 Here, we summarize the results of an interdisciplinary project where we aimed at exploring the origin
85 of tunnel valleys or overdeepenings using a combination of data collected through a gravimetry survey
86 (Bandou et al., 2022, 2023), drillings (Reber and Schlunegger, 2016; Schwenk et al., 2022a, b) and
87 dating (Schläfli et al., 2021; Schwenk et al., 2022a). We focus our study on the Bern area situated on
88 the northern margin of the European Alps (Figure 3a). For this region, we draw a map of the bedrock
89 structure combining the results of a gravimetry survey in the region (Bandou et al., 2023) with
90 information obtained through drilling. This map shows that an overdeepened trough or a tunnel valley
91 system, referred to as the Aare main overdeepening (Schwenk et al., 2022), is made up of two basins
92 separated by a bedrock riegel, which itself is cut by one or multiple slot canyons. This structure has a
93 similar geometry as the examples reported from the Alpine valleys, which points to similar processes
94 resulting in their formation.

95

96 **2 Riegels and slot canyons in the Alpine valleys, and overdeepenings in the Bern area**

97 Bedrock swells between neighboring basins are common features in previously glaciated landscapes
98 and have been reported from various regions around the globe (Anderson et al., 2006; Alley, 2019).
99 They are particularly found in the European Alps (see Figure 2, for a few examples), and they have also
100 been detected underneath active glaciers (Feigl et al., 2018; Nishiyama et al., 2019). In the Alps, most
101 of the bedrock swells occur at the base of valleys (Figure 2) and are dissected by inner gorges or slot
102 canyons that connect the upstream with the downstream basin (Hantke and Scheidegger, 1973; Valla et
103 al., 2009; Montgomery and Korup, 2011). In addition, the Alpine bedrock riegels have a geometry
104 where the upstream stoss side is flatter and has thus a lower dip angle than the downstream lee side.
105 This is particularly the case for the swell in (Figure 2): the Aare valley (Figure 2a; dip of stoss side and
106 lee sides $<5^\circ$ and $>6^\circ$, respectively; Hantke and Scheidegger, 1973), the Trift valley (Figure 2b; c. 30°
107 versus 40° ; Steinemann et al., 2021), the Maggia valley (Figure 2e; 6° versus 40°), and the downstream
108 end of the Urbach valley (Figure 2f; c. 20° versus 6°). In this work, we will document that the
109 overdeepening beneath the city of Bern shares the same geometric properties as the ensemble of bedrock
110 riegels and slot canyons in the Alpine valleys.

111 The target overdeepening near Bern was sculpted by the Aare piedmont glacier with sources in the
112 Central European Alps. From there, the Aare glacier flowed onto the Swiss Plateau over a distance of
113 >20 km, and it merged with the Valais glacier north of Bern, at least during the Last Glacial Maximum
114 (LGM) c. 20 ka ago (Figure 3b). Upstream of the city area of Bern, two bedrock depressions, referred
115 to as the Gürbe tributary channel and the Aare main overdeepening (Figure 3c), form prominent basins
116 that are between c. 150 (Gürbe trough; Geotest, 1995) and >250 m deep (Aare main trough, Kellerhals
117 and Häfeli, 1984) and several kilometers wide (Bandou et al., 2022). Downstream of the city of Bern,
118 the Aare main overdeepening splits into several distributary branches. Among these, the Bümpliz
119 channel ('Bü' in Figure 3c) is the most prominent one with a depth >200 m (Schwenk et al., 2022a, b).

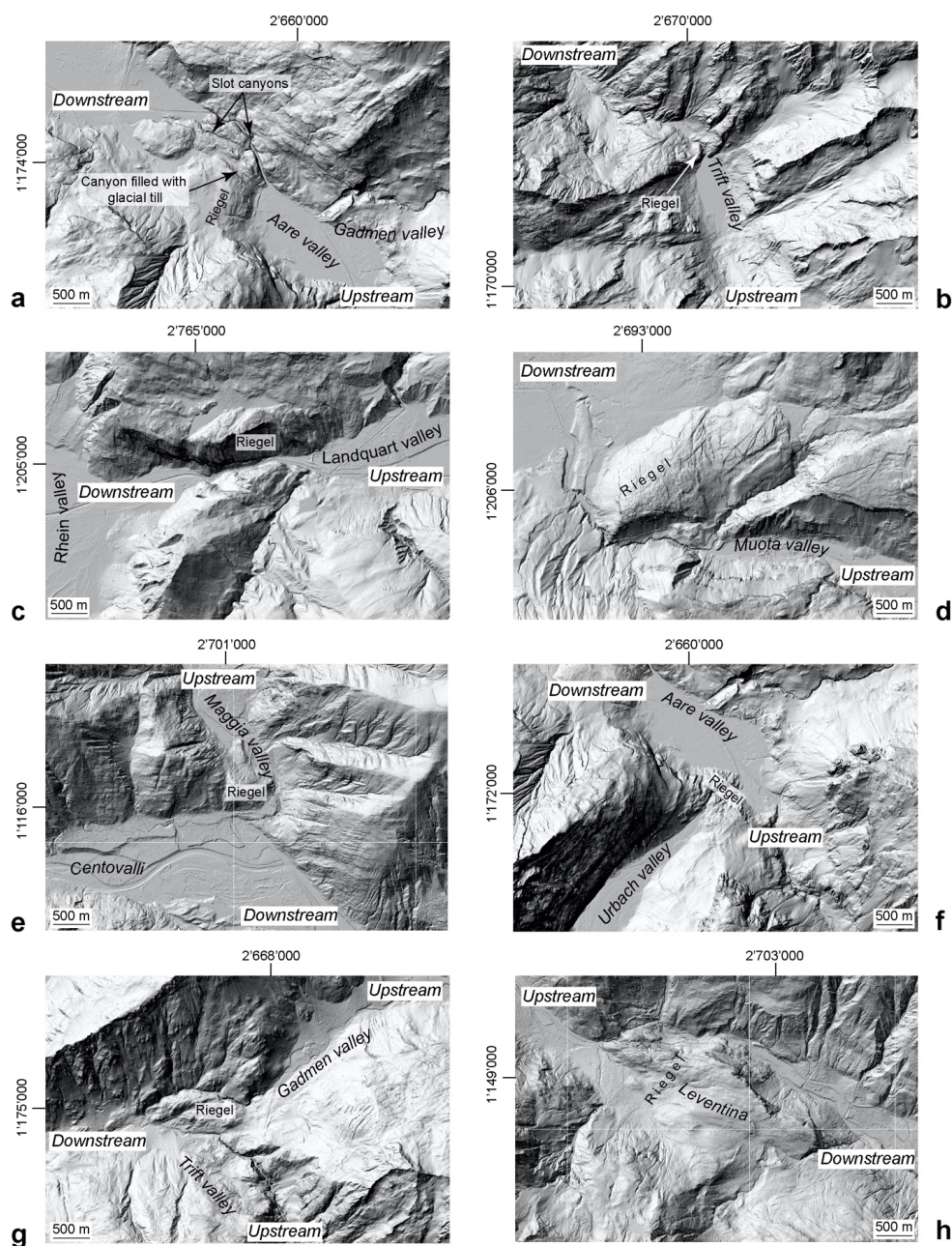


Figure 2

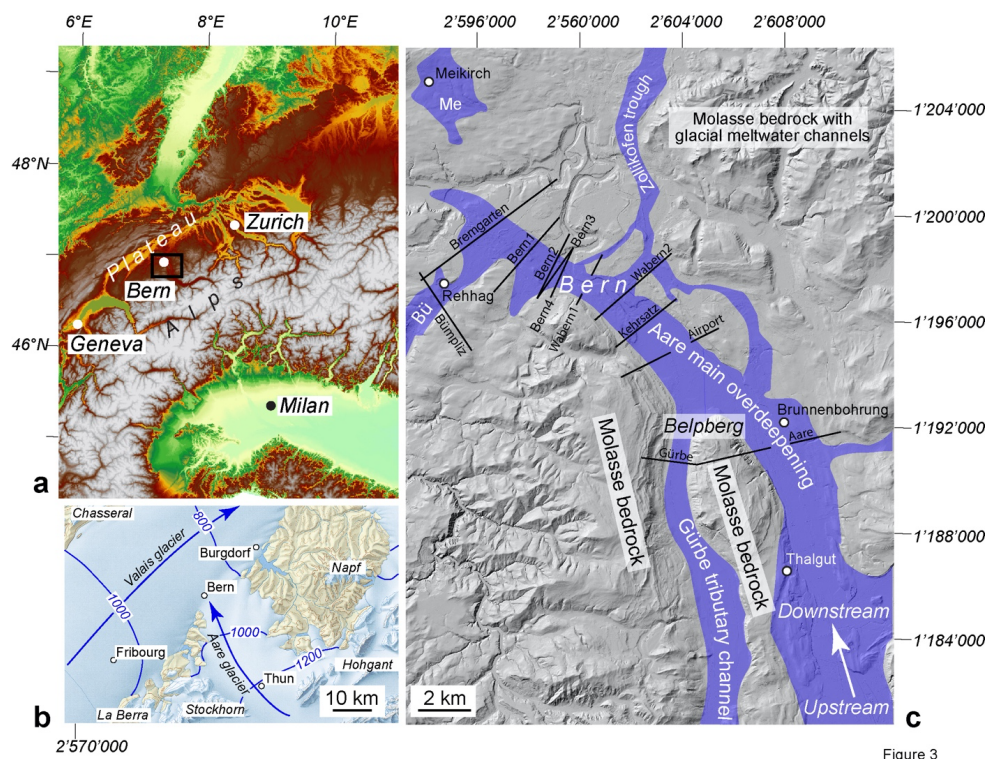
120

Figure 2: Hillshade 2-m-SwissAlti3D DEM (© swisstopo) illustrating examples in the Alpine valleys where bedrock riegels separate overdeepened basins situated farther upstream and downstream. The coordinates refer to the Swiss coordinate system.

121



122 The other depressions such as the Zollikofen trough are shallower and reach a depth of <150 m (Reber
 123 and Schlunegger, 2016). The study region also hosts the Meikirch overdeepening (labelled as ‘Me’ on
 124 Figure 3c), a nearly 200 m-deep trough (Dürst Stucki et al., 2010; Dürst Stucki and Schlunegger, 2003),
 125 which appears to be isolated from the rest of the overdeepening system (Reber and Schlunegger, 2016).



126

Figure 3

Figure 3: Local setting illustrating the a) Alpine arc (modified from Bandou et al., 2023) with latitudes and longitudes, b) the study area during the Last Glacial Maximum (LGM; map with isohypses of the glacier’s surfaces taken from Bini et al., 2009), and c) the surface geomorphology (2 m-SwissAlti3D DEM © swisstopo) together with the orientation of the Aare main overdeepening, taken from Reber and Schlunegger (2016). The figure c) shows (i) the sections along which gravity data was collected (black lines; Bandou et al., 2022; 2023), and (ii) the sites (white circles) where sediments in drillings (Rehhag: Schwenk et al., 2022a, b; Meikirch: Welten, 1982; Preusser et al., 2005; Schläfli et al., 2021; Brunnenbohrung: Kellerhals and Häfeli, 1984; Zwahlen et al., 2021) and exposures (Thalgut: Welten, 1982; 1988; Schlüchter, 1989; Preusser and Schlüchter, 2004) were either dated with various techniques, or where existing ages were reconfirmed by a subsequent analysis. Me=Meikirch overdeepening; Bü=Bümpliz trough. The numbers along the figure margin refer to the Swiss coordinate system (CH1903+).

127

128 Because the area between the northern termination of the Aare main overdeepening and the Meikirch
 129 trough is made up of exposed bedrock (Gerber, 1927), a connection between both depressions was ruled
 130 out (Reber and Schlunegger, 2016). The Aare main overdeepening itself is the most prominent trough
 131 in the city area of Bern and has a maximum depth of nearly 250 m (Reber and Schlunegger, 2016).
 132 The bedrock in the region comprises an amalgamated suite of Early Miocene Upper Marine Molasse
 133 (UMM) sandstone beds south of Bern. Sedimentological analyses showed that these sediments were



134 deposited in a shallow marine, mostly coastal environment (Garefalakis and Schlunegger, 2019). In the
135 region north of Bern, the bedrock is made up of a Late Oligocene to Early Miocene suite of Lower
136 Freshwater Molasse (LFM) sandstones and mudstones (Isenschmid, 2019). These sediments were
137 originally deposited in a fluvial environment (Platt and Keller, 1992; Isenschmid, 2019). The contact
138 between the UMM and the LFM gently dips towards the south (Isenschmid, 2019), with the
139 consequence that south of Bern, the base of the Aare main overdeepening might consist of LFM
140 deposits, while most of the upper part of the overdeepening is laterally bordered by bedrock of the
141 UMM.

142

143 **3 Dataset and Methods**

144 *3.1 Compilation of gravity data*

145 The bedrock topography underneath the city area of Bern was already reconstructed in 2010 and then
146 updated in 2016 based on information retrieved from thousands of drillings that is available from the
147 Geoportal of the Canton Bern (Dürst Stucki et al., 2010; Reber and Schlunegger, 2016). Whereas such
148 information yielded highly resolved spatial information on the bedrock geometry, particularly on its
149 shallower <50 m-deep part (Reber and Schlunegger, 2016), reconstructions of the details for the deeper
150 and thus central part of the Aare main overdeepening have been thwarted because of a lack of drilling
151 information at that time. Here, we benefit from the results of a recent gravity survey conducted in the
152 city area of Bern and information of new drillings >50 m deep (Bandou et al., 2023; Figure 3c). In
153 particular, Bandou et al. (2023) measured the Bouguer gravity anomalies along 10 sections (black lines
154 in Figure 3c). The obtained values were then subtracted from the regional gravity field yielding a
155 residual gravity anomaly value at each site where gravity data was collected. Note that the Quaternary
156 deposits and thus the overdeepening fill has a lower bulk density than the Oligo-Miocene sediments
157 forming the bedrock in the region (Schwenk et al., 2022a; Bandou et al., 2022). Therefore, the
158 occurrence of Quaternary sediments overlying an overdeepened trough result in a negative residual
159 gravity anomaly (Kissling and Schwendener, 1990). Accordingly, a larger bulk mass of Quaternary
160 sediments yields a stronger (and thus a more negative residual anomaly) signal than a fill with less
161 Quaternary material (Kissling and Schwendener, 1990; Bandou et al., 2022). Following this concept,
162 we compiled the residual anomaly data from Bandou et al. (2023) for each gravity profile and drafted a
163 contour map where each line displays the same residual anomaly value. This map (Figure 4a) was drawn
164 by hand, thereby considering the a-priori information about the orientation of the Aare main
165 overdeepening (Reber and Schlunegger, 2016).

166

167 *3.2 Estimating the general shape of the bedrock topography*

168 For a selection of 6 cross-sections along which the residual gravity anomalies were well constrained,
169 Bandou et al. (2023) reconstructed the cross-sectional shape of the overdeepenings using a 3D gravity



170 software referred to as PRISMA (Bandou, 2023). This program uses multiple right-handed prisms to
171 predict the gravity effect of a given structure underneath a point of interest. It bases on an analytical
172 solution by Nagy (1966) and Banerjee and DasGupta (1977) and was conceptualized (Bandou, 2023)
173 to model the general shape of an overdeepening fill. Upon applying this model, Bandou et al. (2023)
174 particularly considered geophysical and geological a-priori information such as the residual gravity
175 anomalies, the density contrasts between the bedrock and the Quaternary fill, the depth of bedrock
176 encountered in drillings, and the already existing bedrock topography model by Reber and Schlunegger
177 (2016). Here, we used the depth of the bedrock as unraveled upon applying the PRISMA routine
178 (Bandou, 2023) to reconstruct the general course of the isohypses (i.e. the lines of constant elevation)
179 of the bedrock underneath the city area of Bern (Figure 4b). Upon drawing this map, we considered that
180 a trend towards less negative residual anomalies points towards a shallowing of the bedrock (Kissling
181 and Schwendener, 1990; Bandou et al., 2023).

182

183 3.3 *Combining the results of the gravity survey with drilling data to reconstruct the details of the* 184 *bedrock topography*

185 We used the existing bedrock topography map of Reber and Schlunegger (2016) as a basis where the
186 isohypses were originally drawn every 10 meters, thereby using the information of thousands of
187 drillings in the region. Because these drillings mainly penetrated the entire Quaternary sequence at the
188 lateral margins of the Aare main overdeepening, the reconstruction of the shallower parts of the bedrock
189 trough is precise. We updated this existing map with information about the general shape of the
190 overdeepening retrieved through the gravity data by Bandou et al. (2023) (Figure 4), and we additionally
191 considered the information of >100 drillings that were sunk >50 m deeply into the subsurface during
192 the past years (Figure 5). Similar to Reber and Schlunegger (2016), we draw the isohypses by hand
193 thereby inferring that changes in the direction of the contour lines and the depths of the bedrock were
194 gradual. We finally combined the map displaying the geometry of the bedrock underneath the
195 overdeepening with the elevation data offered by the 2 m-SwissAlti3D DEM (based on LIDAR data of
196 swisstopo) to present the shape of the bedrock topography as shaded relief. We finally used this map as
197 a basis to draw the cross-sections displayed in Figures 6 and 7.

198

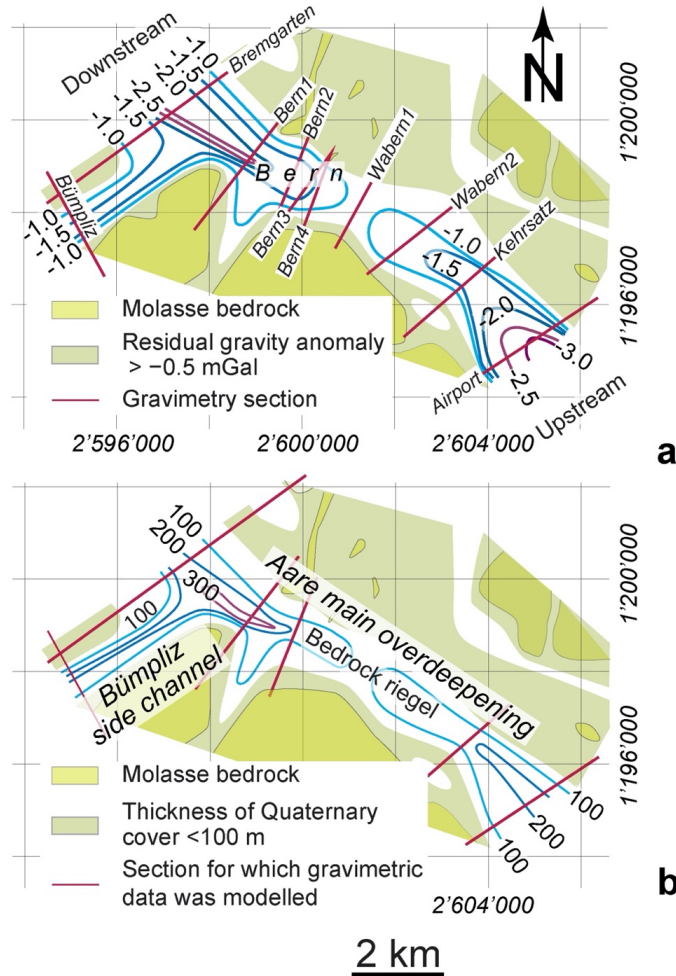
199 **4 Results**

200 4.1 *Patterns of residual gravity anomalies*

201 Based on the results of a gravity survey, Bandou et al. (2022; 2023) showed that the Quaternary fill of
202 the Aare main overdeepening results in a residual gravity anomaly signal that ranges between c. -4.0
203 and -0.5 mGal. In addition, they showed that the gravity signal of the Quaternary fill has a pattern with
204 a distinct change from upstream to downstream. In particular, along the Gürbe-Aare transect (Figure
205 3c), which also crosses a mountain ridge (Belpberg) made up of Molasse bedrock, the corresponding



206 maximum residual anomalies signal ranges from c. -2.9 mGal in the Gürbe valley to c. -4.1 mGal in the
207 Aare valley (Bandou et al., 2022). Farther downstream, the signals of the overdeepening fill decreases,
208



209

Figure 4

Figure 4: Residual gravity anomalies and inferred thicknesses of Quaternary sediments. a) The contour lines of the residual gravity signals (mGal) caused by the Quaternary fill of the Aare main overdeepening are mainly based on gravity surveys along 10 sections (red lines; Bandou et al., 2023). Here, more negative values imply a greater gravity signal and thus a larger bulk mass of Quaternary sediments overlying the overdeepened trough (Kissling and Schwendener, 1990; Bandou et al., 2022). b) Spatial distribution of Quaternary sediments, here expressed by the related thickness pattern. These are mainly based on the results of gravity modelling, where Quaternary mass and its spatial distribution was forward modelled until a best-fit between the modelled and observed gravity signals of the Quaternary mass overlying the overdeepened trough was reached (Bandou, 2023; Bandou et al., 2023). Note that only the residual gravity anomalies of the Airport, Kehrsatz, Bern4, Bern2, Bremgarten and Bümpliz sections were modelled by Bandou et al. (2023). The grid refers to the Swiss coordinate system (CH1903+).

210



211 and the corresponding values change from c. -3.0 mGal (Airport profile) to approximately -1.5 and
212 finally c. -1.0 mGal along the Kehrsatz and Wabern2 profiles, respectively (Figure 4a). The lowest
213 residual anomaly signal with values between c. -0.5 mGal and -1 mGal were reported for the Wabern1
214 profile (Bandou et al., 2023; Figure 3a). Farther downstream, the gravity signal related to the Quaternary
215 fill increases again and reaches values between c. -1.0 and c. -2.0 mGal along the Bern sections, and
216 then approximately -2.5 mGal along the Bremgarten section c. 2 km farther downstream. The residual
217 anomaly data collected along the aforementioned gravity sections thus clearly depict the course of the
218 Aare main overdeepening, which strikes SE-NW in the city area of Bern (Figures 3c, 4a). Towards the
219 NW margin of the study area, a second overdeepening referred to as the Bümpliz side channel (Schwenk
220 et al., 2022b) strikes SW-NE and converges with the Aare main overdeepening NW of Bern. The gravity
221 signal of the Bümpliz sedimentary fill is less and reaches a value of c. -1.5 mGal (Figure 4a; Bandou et
222 al., 2023).

223

224 4.2 *The thickness pattern of Quaternary sediments*

225 The thickest Quaternary suite can be found upstream and downstream of Bern (Figure 4b), where the
226 Aare main overdeepening is between 4 and 5 km wide and > 200 m deep, consistent with drilling
227 information (Bandou et al., 2023). In the city area of Bern, however, the main trough tends to become
228 shallower. This is indicated by the thickness of the Quaternary sediments which becomes 100 m and
229 possibly less (Figure 4b). We acknowledge that further 3D-gravity modelling would be needed to
230 definitely verify such a claim. Although the data cover is low in this zone, the depth versus residual
231 anomaly conversion could be constrained from nearby tie points. Accordingly, the resulting map
232 displaying the thickness pattern of the Quaternary sediments suggests that the bedrock is situated at
233 deeper levels forming a basin on either side of Bern, and that both depressions are separated by a
234 bedrock swell or a riegel that is c. 150 m high but still buried by >100 m of Quaternary sediments
235 (Figure 4b). Finally, the upstream side of the bedrock riegel dips gentler than the downstream side,
236 which is twice as steep: on the stoss side, the residual gravity anomalies change from <-2.5 mGal to >-
237 1.0 mGal over a downstream distance of c. 4 km whereas on the lee side, the same change in the gravity
238 signal occurs over only 2 km. Given that the residual gravity signal is a direct response of the bulk mass
239 of Quaternary sediments overlying the Molasse bedrock, and thus their volume supposing a lower
240 density than the Molasse bedrock (Bandou et al., 2022; 2023), the differences in the upstream and
241 downstream gradients of the residual gravity anomaly values disclose the contrasts in the dip angles of
242 the bedrock topography.

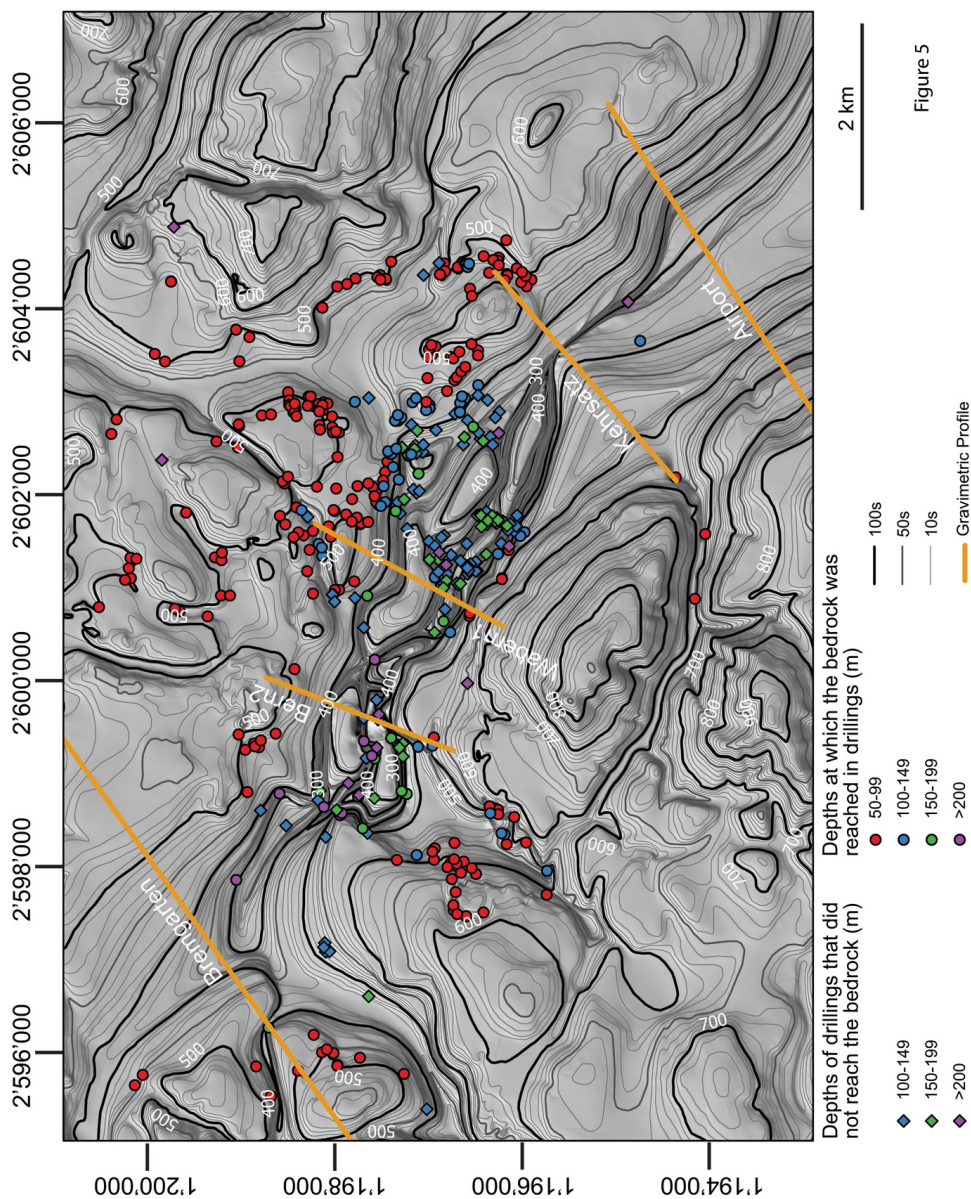
243

244 4.3 *The consideration of deep drillings discloses the occurrence of slot canyons*

245 The reconstructed bedrock topography of the target region reveals a complex pattern (Figure 5), which
246 can be described as a bedrock riegel that is dissected by multiple, partly anastomosing slot canyons or



247 inner gorges (Bandou et al., 2023). At this stage, we cannot precisely reconstruct the number of the
248 inferred canyons because we lack a high-resolution database of deep drillings (Figure 5). Yet, the
249 discrepancy (Figure 6) between (i) a relatively low gravity signal particularly between the Wabern2 and
250 the Bern sections (Figure 4a) and (ii) several drillings that reached the bedrock at much deeper levels
251 that are >200 m below the surface (Figures 5, 6) can only be resolved by invoking the occurrence of a
252 plateau at shallow elevations that is dissected by one or multiple slot canyons. These gorges are up to
253 150 m deep and appear to connect the overdeepened basins upstream and downstream of the city area
254 of Bern. In particular, south of Bern along the Aare profile (Figures 3b and 7a), the Aare main
255 overdeepening is U-shaped in cross-section and displays two levels, each of which with steep lateral
256 flanks and a flat base. While the upper flat base occurs at an elevation of c. 450 m a.s.l., the lower flat
257 contact to the bedrock is situated at c. 250 m a.s.l. and thus approximately 200 m deeper than the upper
258 level (Bandou et al., 2022). Approximately 5 km farther downstream along the Airport section (Figures
259 3b, 7b), the cross-sectional geometry of the Aare main overdeepening maintains its generally U-shaped
260 geometry with a base at an elevation between 200 and 250 m a.s.l. There, the base of the overdeepening
261 appears less flat than farther upstream, but we acknowledge that the density of drillings in the region
262 (Figure 5) and the resolution of the gravity data (Figure 4a, Bandou et al., 2023) is not high enough to
263 fully support this comparison. Upon approaching the city area of Bern, the base of the bedrock becomes
264 shallower and appears to evolve towards a plateau particularly between the Kehrsatz and Bern2 sections
265 (Figures 5, 6, 7c, d and e). This plateau is situated at an elevation of c. 400 m a.s.l. (dashed lines on
266 Figure 7) and dissected by multiple slot-canyons, some of which are up to 150 m deep and too narrow
267 to be detected by the gravity survey (Bandou et al., 2023). Farther to the Northwest reaching the terminal
268 part of the Aare main overdeepening (Figure 3b), the trough widens again and gives way to a relatively
269 deep basin where the deepest part occurs at an elevation of 300 m a.s.l. and possibly even deeper
270 (Figures 5, 7f). This terminal basin appears to be connected with the Bümpliz side channel farther to
271 the SW. Yet the density of drillings is too low (Figure 5) to determine whether a possible bedrock swell
272 separates the Aare main overdeepening from the Bümpliz tributary channel (Figure 3b).



273

Figure 5: Hillshade DEM, illustrating the bedrock topography of the Bern area, together with deep drillings that either reached the bedrock (circles) or that ended in Quaternary sediments (diamonds). The shallow drillings (<50 m) are not displayed on this map since the number is too large (more than 1000, please see Reber and Schlunegger, 2016). The isohypses were drawn for every 10 meters. The coordinates along the figure margin refer to the Swiss coordinate system (CH1903+). The sections shown on this map are used to illustrate the cross-sectional geometry of the overdeepening beneath Bern (see next figures).

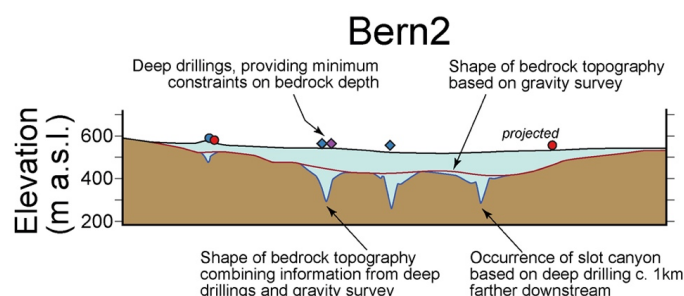
274



275 **5 Discussion**

276 *5.1 Subglacial origin and the role of subglacial meltwater*

277 It is agreed upon in the literature that the formation of overdeepened basins can be understood as the
 278 response of erosion by glaciers. As summarized in Figure 1, the main arguments that have been put
 279 forward are (i) the depth of the base of these depressions, which are generally located below the current
 280 fluvial base-level, and (ii) the occurrence of adverse slopes in the downstream direction of these basins
 281 (Preusser et al., 2010; Patton et al., 2016; Alley et al., 2019; Magrani et al., 2022; Gegg and Preusser,
 282 2023). As outlined in the previous sections, such geometric features are also encountered for the Aare
 283 main overdeepening beneath the city of Bern. Therefore, it is not surprising that the origin of this
 284 depression has repeatedly been interpreted as the response of the erosional processes of a glacier with
 285 a source in the Central Alps of Switzerland (Dürst Stucki et al., 2010; Preusser et al., 2010; Reber and
 286 Schlunegger, 2016; Magrani et al., 2022; Bandou et al., 2023). Furthermore, as already outlined by
 287 Bandou et al. (2023) and further detailed in this work, the overdeepening underneath Bern can
 288 additionally be subdivided into a southeastern and a northwestern sub-basin. These depressions are
 289 separated from each other by a bedrock riegel or swell, which itself is dissected by one or multiple slot
 290 canyons establishing a hydrological link between the upstream and downstream basins (Figures 1, 5
 291 and 7).



292

Figure 6

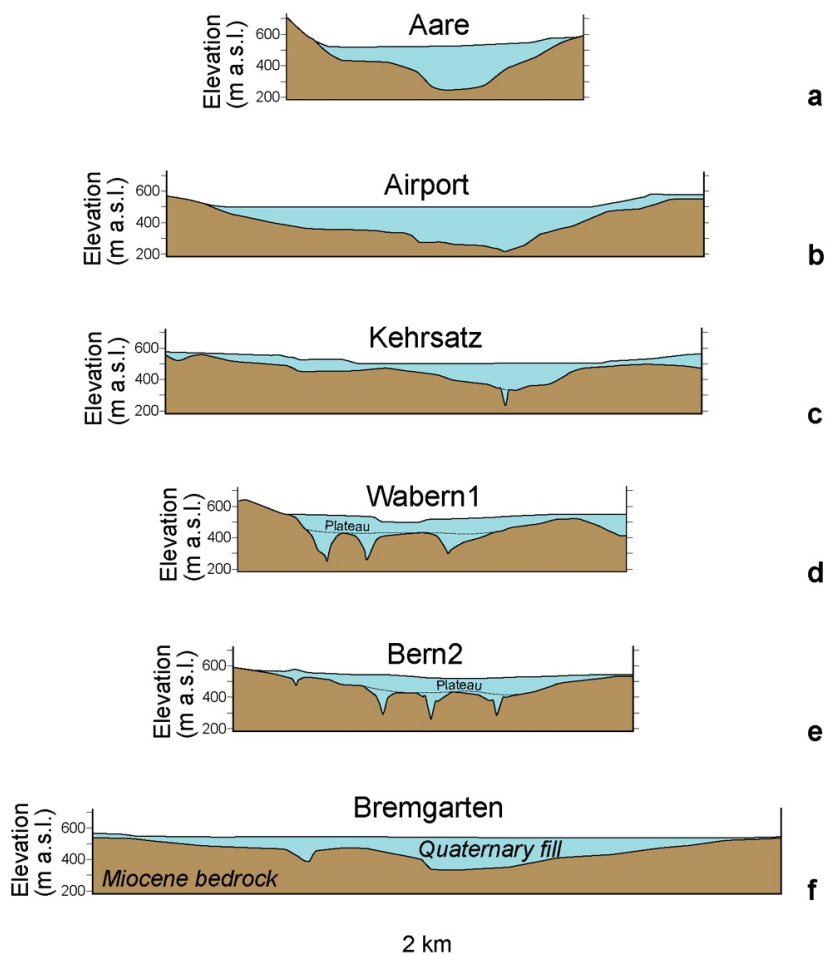
Figure 6: Example that illustrates of how we proceeded upon reconstructing the bedrock topography beneath Bern. We started with the general shape of the bedrock topography using the gravity signal of the bulk Quaternary mass as a basis (red line, and Figure 4b). Information from drillings >50 m deep (circles and diamonds: see Figure 5 for explanation of colors) allowed then to reconstruct the course and geometry of the slot canyons (blue line). The mass of their Quaternary fill is too low to be identified by the gravity survey. This is the case because the strength of a gravity signal decays exponentially with depth (see also Bandou et al., 2023, for further

293

294 Using geomorphic evidence in combination with information about rates of rock uplift and fluvial
 295 incision into bedrock, Montgomery and Korup (2011) argued that an ensemble of bedrock riegels and
 296 slot canyons were shaped over several glacial/interglacial periods, and that they were most likely formed
 297 by subglacial meltwater during the decay of the glaciers and ice caps, when large volumes of meltwater
 298 were released. Such processes were particularly invoked to explain the history of inner gorge formation



299 in the Landquart and the Trift valleys (Figures 6b, 6c) situated in the Swiss Alps (Montgomery and
300 Korup, 2011; Steinemann et al., 2021).



301

Figure 7

Figure 7: Sections through the Bern area, where the geometry of the bedrock is taken from the DEM illustrated in Figure 5. The Aare section is taken from Bandou et al. (2022). See Figures 3 and 5 for location and orientation of sections.

302

303 As further examples, erosion by subglacial meltwater was put forward to explain the occurrence of inner
304 gorges at the margin of the Fennoscandian ice sheet (based on the pattern of surface exposure ages;
305 Jansen et al., 2014) and such a mechanism was used to explain (i) the origin of the deep channels on
306 the floor of the eastern English Channel, and (ii) the breaching of the bedrock swell at the Dover strait
307 during the aftermath of the Marine Isotope Stage (MIS) 12 or a later glaciation (Gupta et al., 2007;
308 Cohen et al., 2014; Gupta et al., 2017). In this context, Jansen et al. (2014) noted that a typical field
309 evidence for inferring a subglacial meltwater control includes (i) the occurrence of anastomosing



310 channels, (ii) undulating valley long profiles, and (iii) a topography that apparently amplifies the
311 hydraulic potential. The resolution of our data is at a larger scale than the thalweg irregularities, but
312 sufficient to display the anastomosing patterns of the slot canyons, with channels meandering, splitting
313 and merging again (Figure 5).

314

315 5.2 *Formation through erosion by subglacial meltwater inferred from theory and modelling*

316 A subglacial meltwater contribution to the controls on the formation of overdeepenings was inferred
317 based on theoretical relationships between meltwater runoff and the sediment transport capacity of
318 proglacial and subglacial streams (e.g., Boulton and Hindmarsch, 1987; Alley et al., 1997; Herman et
319 al., 2011, Beaud et al., 2016). Because sediment transport increases exponentially with both the amount
320 and seasonality of meltwater runoff, Alley et al. (1997) interpreted that subglacial and proglacial
321 streams are among the most efficient sediment-transport mechanisms on Earth. This process peaks in
322 the ablation zone of a glacier, where surface melt reaches the bed and significantly contributes to the
323 generation of subglacial runoff. Yet, subglacial meltwater appears to play a minor role in contributing
324 to a sedimentary budget if the subglacial runoff has a negligible contribution from surface melt (Alley
325 et al., 1997). Finally, Cohen et al. (2023) showed that subglacial water is able to remove the sediment
326 from the base of a glacier and to further incise into bedrock provided that the pressure of the subglacial
327 meltwater and that of the ice overburden is at least the same, as also put forward by Boulton and
328 Hindmarsch (1987). The results from the model of Cohen et al. (2023), tailored to determine the location
329 of the subglacial drainage pathways, further suggest that such conditions most likely prevailed at the
330 front of piedmont glaciers and particularly during the decay when large volumes of meltwater were
331 available. In addition, the model predicts that under such circumstances, the locations of subglacial
332 meltwater pathways are likely to coincide with segments where high rates of glacial erosion occur
333 (Cohen et al., 2023). Therefore, it is not surprising that reaches with evidence for intense erosion by
334 both water and ice occur in the same area and are hydrologically connected with each other, as is the
335 case for the ensemble of overdeepened basins and slot canyons beneath Bern. Yet besides hydrological
336 conditions, the erosional resistance of bedrock plays an important role where a bedrock swell could
337 potentially form. This aspect is elaborated in the following paragraph.

338

339 5.3 *The role of bedrock strength*

340 The formation of riegels and basins is consensually understood as conditioned by differences in bedrock
341 strengths. This also concerns the controls on the size of a basin itself where bedrock with a low erosional
342 resistance tends to host a larger basin than lithologies where the erosional resistance is high (e.g.,
343 Magrani et al., 2020; Gegg and Preusser, 2023). Following this logic, swells preferentially form in
344 locations where the bedrock has a lower erodibility than the rock units farther upstream and
345 downstream. This has been documented for the riegel in the Trift valley (Figure 2a), which separates



346 an overdeepened basin upstream from a wide valley farther downstream (Steinmann et al., 2021).
347 There, the bedrock forming the ridge is made up of a banded, biotite-rich gneiss (Erstfeld gneiss),
348 whereas the bedrock upstream and downstream of the swell is cut by multiple faults and fractures, thus
349 offering a lower resistance to erosion. As another example, the bedrock riegel downstream of the
350 confluence between the Aare and Gadmen valleys (Figure 2a) is made up of the Quinten Formation
351 (Stäger et al., 2020). These limestones tend to have a higher mechanical strength (Kühni and Piffner,
352 2001) than the sandstones-marl alternations (North Helvetic Flysch; Stäger et al., 2020) downstream of
353 the bedrock swell, and the suite of sandstones, marls and dolomite beds upstream of it (Mels- and
354 Quarten Formations; Stäger et al., 2020). In the Bern area, the inferred riegel is underlain by Late
355 Miocene shallow marine sandstone (i.e. UMM), whereas the bedrock farther downstream comprises a
356 suite of Late Oligocene fluvial sandstones (i.e. LFM) and marl interbeds (Isenschmid, 2019). It is
357 postulated that the UMM sediments have a higher erosional resistance than the underlying LFM unit,
358 based on the observation that the UMM forms a cap rock in the region (Isenschmid, 2019). Accordingly,
359 the bedrock architecture in the Bern area is comparable to the examples explained above where the
360 UMM bedrock forming the swell has a larger erosional resistance than the LFM units at least
361 downstream of the riegel (Isenschmid, 2019). It is possible that Lower Freshwater Molasse (LFM)
362 deposits with a low erosional resistance also occur at the base of the overdeepening farther upstream of
363 the swell. We infer this from the Gurten drilling on the SW margin of the Wabern1 profile (Figure 4)
364 where the LFM bedrock was encountered at a depth of >300 m a.s.l. (Garefalakis and Schlunegger,
365 2019). This is indeed shallower than the basal part of the Aare main overdeepening along e.g., the
366 Airport profile (Figure 6b).

367 Presumably more important than the contrasts in bedrock erodibility: the bedrock swell underneath Bern
368 is situated just upstream of the confluence area between the Valais and Aare glaciers (Figure 3b). As
369 such, this situation shares many similarities with the examples in the Alpine valleys where the bedrock
370 swells are situated directly upstream (Figures 2c, 2d, 2e and 2f), directly downstream (Figures 2a, b) or
371 at the confluence (Figures 2g, h) between a tributary and a trunk valley. In the same sense, Lloyd et al.
372 (2023) found that overdeepened basins and, as a consequence, the occurrence of bedrock swells farther
373 downstream, are mainly situated in the confluence area of glacial valleys. In this case, the deep carving
374 into the bedrock would be the result of an acceleration of the ice flow in response to the increase in the
375 ice flux downstream of the confluence region (Herman et al., 2015). Alternatively, a bedrock riegel
376 could also form upstream of the confluence of two glaciers as is the case in the Maggia and Urbach
377 valleys (Figure 2e, f). Such a situation most likely also prevailed in the Bern area, at least during LGM
378 times. There, the damming of the Aare glacier by the much larger Valais glacier could have caused a
379 reduction of the flow velocity of the Aare glacier (Figure 3b). Consequently, the shear velocity and thus
380 the bedrock abrasion rates would decrease, thereby facilitating the preservation of a bedrock swell.

381



382 *5.4 Differences in the geometries between the exposed riegels and basins in the Alpine valleys, and*
383 *the overdeepening beneath Bern*

384 Despite obvious similarities, there are also major differences between the geometric properties of the
385 overdeepening system beneath Bern and the currently exposed riegels and slot canyons in the Alpine
386 valleys (Figure 2 versus Figures 5 and 7). The most striking one is the occurrence of the riegel and inner
387 gorges approximately 50-100 m below the current base-level, and the absence of an obvious
388 continuation of the thalweg NW of Bern (Figure 3c). It is indeed very unlikely that the Aare main
389 overdeepening was linked with the Meikirch depression farther to the north (Figure 3c). We base this
390 interpretation on available geological maps (Gerber, 1927) and drillings (Reber and Schlunegger, 2016),
391 showing that the northern edge of the Aare main overdeepening and the Meikirch trough are separated
392 by Molasse bedrock with no evidence for connecting channels. Accordingly, the inferred interpretation
393 where the slot canyons beneath Bern were formed by subglacial meltwater requires a mechanism where
394 the meltwater is not only capable to incise into bedrock beneath a glacier, but also to escape the
395 depression by ascending nearly 200 m from the base of the overdeepening to the surface near the
396 glacier's snout. Using Bernoulli's principle as a basis (e.g., Batchelor, 1967), it was proposed that such
397 an ascent of subglacial meltwater was driven by the translation of large hydrostatic pressures into
398 hydrodynamic pressures at the downstream margin of a glacier (Dürst Stucki and Schlunegger, 2013).
399 In addition, such a mechanism is most effective at work where the surface slope of a glacier is steeper
400 than the adverse slope of an overdeepening (Hooke and Pohjola, 1994), as is commonly found in the
401 frontal part of a glacier (Figure 1a). Since the ratio between the densities of ice and water is >0.9
402 (Harvey, 2007), the inferred 200 m-rise of the meltwater requires a minimum hydrostatic pressure
403 corresponding to >250 m-thick ice to allow an upward water flow, and it conditions the occurrence of
404 a hydrologically closed subglacial channel network. Such a scenario is realistic, as in the Bern area the
405 Aare glacier was several hundred m thick during the past glaciations (Bini et al., 2009; Preusser et al.,
406 2011; Figure 3b). If this hypothesis is valid, then the thickness of the piedmont glaciers sets an
407 uppermost limit to the depth at which overdeepenings can be carved into the bedrock, mainly because
408 sufficient pressures are required for the subglacial meltwater to ascend to the surface from deeper levels.
409 Yet it is possible that the large porosities of nearly 20% in the Molasse sandstones (Keller et al., 1990)
410 could have facilitated the escape of subglacial meltwater to the groundwater. This could have caused a
411 reduction in static pressures, violating the inference of a closed system. However, we consider the
412 permeabilities of the Molasse sandstone beds (<1000 md, Keller et al., 1990) as low enough to consider
413 depressurization through meltwater runoff to the groundwater as negligible.

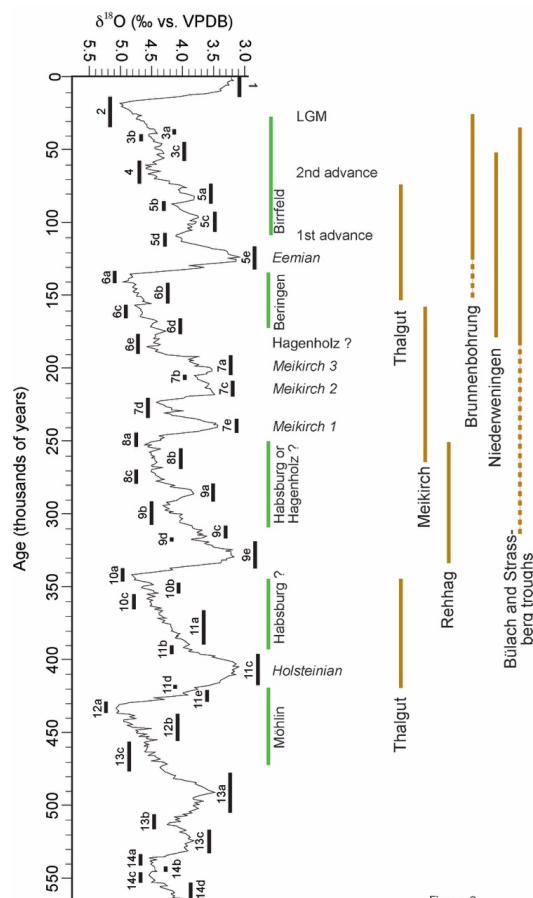


Figure 8

414

Figure 8: Development of stable isotopes and Marine Isotope Stages (MIS) within a chronological framework (Lisiecki and Raymo, 2005; Railsback et al., 2015) and glacial periods recorded in the Plateau of the Swiss Alps (modified after Preusser et al., 2011; 2021). The age of the Möhlín glaciation is taken from Dieleman et al. (2022). The age of the Thalgut section is based on pollen records (Welten, 1982; 1984) and was subsequently described by Schlüchter (1989), yielding a Holsteinian age for the basal part of the section. The chronological framework for the upper part of this section was then updated by Preusser and Schlüchter (2004). The Holsteinian could either correspond to MIS 9 (according to U/Th ages established for peat layers in the type section of the Holsteinian at Bossel, Germany; Geyh and Müller, 2005) or to MIS 11 based on $^{40}\text{Ar}/^{39}\text{Ar}$ ages of tephra (Roger et al., 1999). Following Koutsodendris et al. (2012) we preferentially use an age assignment to MIS 11. Ages for the Meikirch section are based on pollen assemblages (Welten, 1982) and optically stimulated luminescence (OSL) ages by Preusser et al. (2005). The pollen assemblages of Welten (1982) were subsequently reinterpreted by Schläfli et al. (2021). The ages of the deposits encountered in the Brunnenbohrung are based on concentrations of ^{14}C measured in organic material at nearly the base of the drilling (Kellerhals and Häfeli, 1984; Zwahlen et al., 2021). The chronological framework of the Rehhag drilling was established by Schwenk et al. (2022a) using the results of feldspar luminescence dating conducted on two samples at the top of a section, which is exposed in a quarry next to the Rehhag drilling. Finally, the chronology of the Niederweningen drilling and sediments encountered in the Bülach and Strassberg troughs are based on OSL signals measured in quartz minerals (Niederweningen: Dehnert et al., 2012; Bülach and Strassberg troughs: Büchi et al., 2018).

415



416 5.5 *Chronological framework*

417 A high-resolution chronological framework (e.g., Reber et al., 2014; Kamleitner et al., 2023a) has been
418 established from deposits of the LGM that occurred c. 20 ka ago (Ivy-Ochs et al., 2008; Kamleitner et
419 al., 2023b) (Figure 7). A relatively detailed chronology is also available for the first and second glacial
420 advances during the Birrfeld glaciation (Ivy-Ochs et al., 2008; Preusser, 2004; Preusser et al., 2007;
421 2011; Pfander et al., 2022). For previous glaciations, the chronological framework is less clear. Yet,
422 Preusser et al. (2011) summarized multiple evidence for proposing that the piedmont glaciers did
423 advance into the Alpine foreland between 185 and 130 ka, i.e. the Beringen glaciation (MIS 6, Figure
424 8), and that this advance into the foreland was larger than during the LGM. The age assignments to the
425 glaciations preceding MIS 6 are still debated. While the largest extent of the north Alpine glaciers (Most
426 Extensive Glaciation of the Swiss Foreland cf. Schlüchter, 1988) was assigned to the Möhlin glaciation
427 (Preusser et al., 2011) and recently dated to 500 ± 100 ka and thus to MIS 12 through burial dating with
428 cosmogenic ^{26}Al and ^{10}Be (Dieleman et al., 2022), a re-evaluation of the reported concentrations of the
429 cosmogenic nuclides yielded an age that is more consistent with MIS 6 (Nørgaard et al., 2023). Yet we
430 favour the chronology by Dieleman et al. (2022) and the assignment to a MIS 12 age because it is better
431 supported by a-priori field-based information such as the results of detailed mapping. The ages of the
432 Habsburg and Hagenholz glaciations, which occurred between the Beringen and Möhlin glaciations,
433 are the least constrained. Whereas Preusser et al. (2011) considered the Hagenholz ice advance to
434 postdate MIS 7 (Figure 8), Büchi et al. (2018) and subsequently Preusser et al. al. (2021) rather
435 considered the Hagenholz glaciation to predate MIS 7 thereby following Keller and Kryass (2010).

436 The Quaternary fill of overdeepenings can now be placed into the aforementioned chronological
437 framework of glacial advances onto the Swiss plateau during the past glaciations (Figure 8). The
438 database is sparse, but the available ages imply that the oldest backfills that have been dated so far
439 postdate the Most Extensive Glaciation (or the Möhlin glaciation), dated to MIS 12 (Figure 8). This is
440 the case for the sedimentary fill of the Aare main overdeepening where the occurrence of a Holsteinian
441 interglacial lacustrine sequence (Figure 8) was reported for the basal marls of the Thalgut section, which
442 could either correspond to MIS 9 (Roger et al., 1999) or MIS 11 (see discussion in Preusser et al., 2011;
443 Koutsodendris et al., 2012; and Schwenk et al., 2022a for discussion of ages). In addition, c. 6 km
444 farther downstream from the Thalgut section, nearly the entire sedimentary sequence of the Aare main
445 overdeepening was encountered in the Brunnenbohrung drilling (Figure 3c) and was constrained to an
446 age postdating MIS 6 (Kellerhals and Häfeli, 1984; Zwahlen et al., 2021). The related sedimentary suite
447 could thus span the entire time interval between the Beringen and Birrfeld glaciations including the
448 Holocene (Bandou et al., 2022). Farther north of Bern, the Quaternary succession overlying the bedrock
449 has an age that is MIS 8 and older (Schwenk et al., 2022a), thus corresponding to the Habsburg
450 glaciation or any other glacial period pre-dating Habsburg (Figure 8). These ages are not precise enough
451 to reconstruct in detail the history of how and particularly when the overdeepenings were formed, but



452 they are consistent with the chronologies established for other overdeepening fills (Figure 8). In
453 particular, most published ages do support an interpretation where the deep troughs were originally
454 formed after the Middle Pleistocene Transition (Schluchter, 2004) and thus during the same period
455 when the U-shaped Alpine valleys were carved (Häuselmann et al., 2007; Valla et al., 2011). This was
456 also the same time when the base-level in the northern margin of the Swiss Plateau lowered at the
457 highest rates (Claude et al., 2019). Apparently, the change in the frequency of glacial-interglacial cycles
458 from a 40 ka- to a 100 ka-periodicity, which occurred c. 800 ka ago, not only resulted in rapid glacial
459 erosion (Pedersen and Egholm, 2013) and in the deep glacial carving of U-shaped valleys in the Alps
460 (Häuselmann et al., 2007, Valla et al., 2011), but also in the formation of overdeepenings with complex
461 geometries including basins, riegels and slot canyons in the foreland.

462

463 **6 Conclusions**

464 Bedrock riegels separating upstream and downstream basins are common features in modern Alpine
465 valleys, and they are likely to be encountered in overdeepenings. In addition, we propose that these
466 riegels occur as ensembles together with slot canyons that cut through the swells and establish a
467 hydrological link between the upstream and downstream basins. We suggest this based on our
468 reconstruction of the bedrock topography of the Aare main overdeepening in the Bern area, and we
469 propose that such ensembles of basins, riegels and slot canyons also occur in other Alpine
470 overdeepenings such as the Rhone, Rhine and Inn valleys (Figure 9). We suggest that these slot canyons
471 were formed through incision by glacial meltwater during the decaying state of a glacier when large
472 volumes of meltwater were available. For the bedrock swell underneath Bern, the resolution of the
473 dataset presented in this work does not allow to locate and reconstruct the precise course of the inferred
474 slot canyons. Yet the presented reconstruction of the bedrock topography does reconcile (i) the
475 occurrence of a low residual gravity anomalies in the Bern area (Figure 4a), which implies a relatively
476 low bulk mass of Quaternary sediments, and (ii) the depth at which Quaternary sediments were
477 encountered in drillings (Figures 5, 6). In addition, in many Alpine valleys, such structures appear to be
478 preferentially formed in the confluence area between two glacial valleys and where the bedrock has a
479 relatively low erodibility. We posit this hypothesis for the overdeepening below the Bern area, where
480 such a bedrock swell appears to be situated just upstream of the confluence between the Aare and Valais
481 glaciers, at least during LGM times and possibly during previous glaciations. In addition, the inferred
482 bedrock riegel beneath Bern is located where the bedrock has a lower erodibility than downstream and
483 possibly upstream, at least in the basal part of the trough. Yet, we acknowledge that an improved
484 understanding about the origin of such structures requires more information particularly on the
485 chronology of glacial advances and the overdeepening fills.

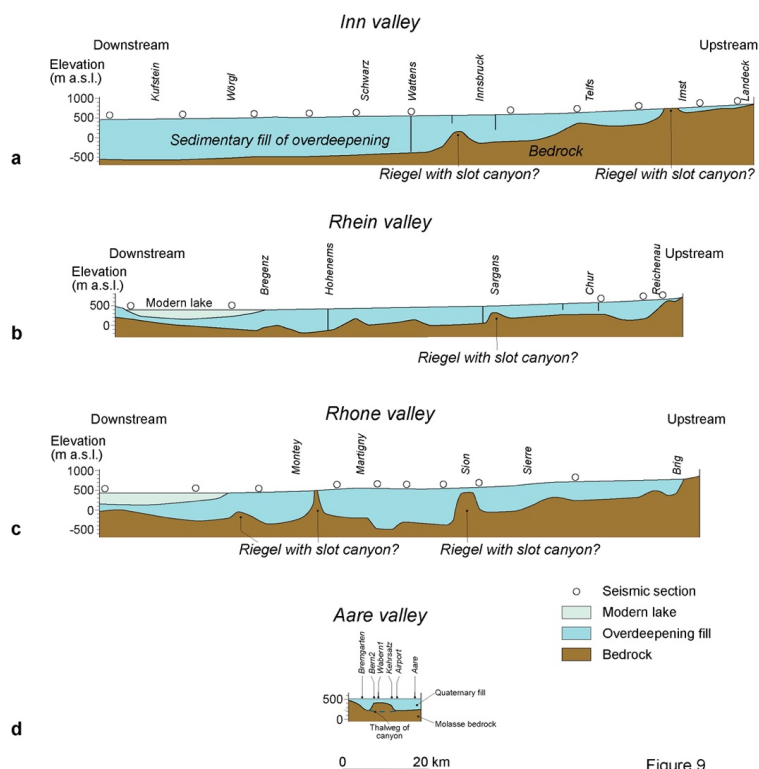


Figure 9

486

Figure 9: Sections showing the patterns of overdeepenings from upstream to downstream for a) the Inn valley, b) the Rhine valley, c) the Rhone valley and d) the Aare valley in Bern area. The examples of the Inn, the Rhine and the Rhone valleys are taken from Hinderer (2001), whereas the section along the Aare valley is a modified version of Bandou et al. (2023) and bases on the data presented in Figure 5. The data from the Aare valley covers a short distance only, but it shows a striking similarity to the riegels in the large Alpine valleys. Therefore, it is quite likely that the other riegels are also dissected by narrow channels and that all settings share a similar origin.

487

488

489 **Acknowledgement**

490 This work was financially supported by the Swiss National Science Foundation (project No.
491 200021_175555) with contributions from the Stiftung Landschaft und Kies, swisstopo and the
492 Gebäudeversicherung Bern GVB.

493

494 **Data availability**

495 All data used in this paper can be ordered by the Authorities of the Canton Bern and by the authors on
496 request.

497

498 **Author contributions**

499 EK designed the study, together with FS and DB. DB collected the gravity data and processed them,
500 with support by UM and EK. FS wrote the paper and conducted the analyses and interpretation of the



501 data. RB drafted the bedrock topography map. PS, MS, DM and GD contributed to the discussion. All
502 authors approved the article.

503

504 **Competing interests**

505 The authors declare that they have no conflict of interest.

506

507 **References**

508 Alley, R.B., Cuffey, K.M., Evenson, E.B., Strasser, J.C., Lawson, D.E., and Larson, G.J.: How glaciers
509 entrain and transport basal sediment: physical constraints. *Quat. Sci. Rev.*, 16, 1017-1038, 1997.

510 Alley, R., Cuffey, K., and Zoet, L.: Glacial erosion: Status and outlook. *Ann. Glaciol.*, 60, 1–13.
511 <https://doi.org/10.1017/aog.2019.38>, 2019.

512 Anderson, R.S., Molnar, P., and Kessler, M.A.: Features of glacial valley profiles simply explained. *J.*
513 *Geophys. Res.*, Earth Surface, 111, F01004, doi:10.1029/2005JF000344, 2006.

514 Anselmetti, F., Bavec, M., Crouzet, C., Fiebig, M., Gabriel, G., Preusser, F., Ravazzi, C., and Dove
515 team.: Drilling Overdeepened Alpine Valleys (ICDP-DOVE): quantifying the age, extent, and
516 environmental impact of Alpine glaciations. *Sci. Drill.*, 31, 51–70. [https://doi.org/10.5194/sd-](https://doi.org/10.5194/sd-31-51-2022)
517 [31-51-2022](https://doi.org/10.5194/sd-31-51-2022), 2022.

518 Bandou, D.: Gravi3D: A 3D forward modelling software using gravity data to resolve the geometry of
519 subsurface objects, <https://zenodo.org/doi/10.5281/zenodo.8153258>, 2023.

520 Bandou, D., Schlunegger, F., Kissling, E., Marti, U., Schwenk, M., Schläfli, P., Douillet, G., and Mair,
521 D.: Three-dimensional gravity modelling of a Quaternary overdeepening fill in the Bern area of
522 Switzerland discloses two stages of glacial carving. *Scientific Rep.*, 12, 1441,
523 <https://doi.org/10.1038/s41598-022-04830-x>, 2022.

524 Bandou, D., Schlunegger, F., Kissling, E., Marti, U., Reber, R., and Pfander J.: Overdeepenings in the
525 Swiss plateau: U-shaped geometries underlain by inner gorges. *Swiss. J. Geosci.*, 116, 19,
526 <https://doi.org/10.1186/s00015-023-00447-y>, 2023.

527 Banerjee, B., and Gupta, S.P.: Gravitational attraction of a rectangular parallelepiped. *Geophysics*, 42,
528 1053–1055, 1977.

529 Batchelor, G. K.: An introduction to fluid dynamics (p. 615). Cambridge Univ. Press, 1967.

530 Beaud, F., Flowers, G.E., and Venditti, J.G.: Efficacy of bedrock erosion by subglacial water flow. *Earth*
531 *Surf. Dyn.*, 4, 125-145, <https://doi.org/10.5194/esurf-4-125-2016>, 2016.

532 Bini, A., et al.: Die Schweiz während des letzteiszeitlichen Maximums (LGM) 1:500'000. Bundesamt
533 für Landestopografie swisstopo, Bern, Switzerland, 2009.

534 Boulton, G.S., and Hindmarsh, R.C.A.: Sediment deformation beneath glaciers: rheology and
535 geological consequences. *J. Geophys. Res.* 92, 9059-9082, 1987.



- 536 Brocklehurst, S.H., and Whipple, K.X.: Glacial erosion and relief production in the eastern Sierra
537 Nevada, California. *Geomorphology* 42, 1–24, 2002.
- 538 Brocklehurst, S.H., Whipple, K.X., and Foster, D.: Ice thickness and topographic relief in glaciated
539 landscapes of the western USA. *Geomorphology*, 97, 35–51,
540 <https://doi.org/10.1016/j.geomorph.2007.02.037>, 2008.
- 541 Büchi, M. W., Frank, S. M., Graf, H. R., Menzies, J., and Anselmetti, F. S.: Subglacial emplacement of
542 tills and meltwater deposits at the base of overdeepened bedrock troughs. *Sedimentology*, 64,
543 685. <https://doi.org/10.1111/sed.12319>, 2017.
- 544 Büchi, M., Graf, H.R., Haldimann, P., Lowick, S.E. and Anselmetti, F.S.: Multiple Quaternary erosion
545 and infill cycles in overdeepened basins of the northern Alpine foreland. *Swiss J. Geosci.*, 111,
546 133–167, <https://doi.org/10.1007/s00015-017-0289-9>, 2018.
- 547 Burschil, T., Buness, H., Tanner, D.C., Wiedlandt-Schuster, U., Ellwanger, D., and Gabriel, G.: High-
548 resolution reflection seismics reveal the structure and the evolution of the Quaternary glacial
549 Tannwald Basin. *Near Surf. Geophys.*, 16, 593–610, <https://doi.org/10.1002/nsg.12011>, 2018.
- 550 Burschil, T., Tanner, D., Reitner, J., Buness, H., and Gabriel, G.: Unravelling the complex stratigraphy
551 of an overdeepened valley with high-resolution reflection seismics: The Lienz Basin (Austria),
552 *Swiss J. Geosci.*, 112, 341–355, <https://doi.org/10.1007/s00015-019-00339-0>, 2019.
- 553 Carter, C.L., and Anderson, R.S.: Fluvial erosion of physically modeled abrasion-dominated slot
554 canyons. *Geomorphology*, 81, 89–113, <https://doi.org/10.1016/j.geomorph.2006.04.006>, 2006.
- 555 Clark, P.U., and Walder, J.S. Subglacial drainage, eskers, and deforming beds beneath the Laurentide
556 and Eurasian ice sheets. *Geol. Soc. Amer. Bull.*, 106, 304–314, [https://doi.org/10.1130/0016-7606\(1994\)106<0304:SDEADB>2.3.CO;2](https://doi.org/10.1130/0016-7606(1994)106<0304:SDEADB>2.3.CO;2), 1994.
- 558 Claude, A., Akçar, N., Ivy-Ochs, S., Schlunegger, F., Kubik, P.W., Christl, M., Vockenhuber, C.,
559 Kuhlemann, A., Rahn, M., and Schlichter, C.: Changes in landscape evolution patterns in the
560 northern Swiss Alpine Foreland during the mid-Pleistocene revolution. *GSA Bull.*, 131, 2056–
561 2078, <https://doi.org/10.1130/B31880.1>, 2019.
- 562 Cohen, K. M., Gibbard, P. L., and Weerts, H. J. T.: North Sea palaeogeographical reconstructions for
563 the last 1 Ma. *Neth. J. Geosci.* 93, 7–29, 2014.
- 564 Cohen, D., Juvet, G., Zwinger, T., Landgraf, A., and Fischer, U.H.: Subglacial hydrology from high-
565 resolution ice-flow simulations of the Rhine Glacier during the Last Glacial Maximum: a proxy
566 for glacial erosion. *E&G Quat. Sci. J.*, 72, 189–201, <https://doi.org/10.5194/egqsj-72-189-201>,
567 2023.
- 568 Cook, S. J., and Swift, D. A.: Subglacial basins: Their origin and importance in glacial systems and
569 landscapes. *Earth-Science Rev.*, 115, 332–372,
570 <https://doi.org/10.1016/j.earscirev.2012.09.009>, 2012.



- 571 Dehnert, A., Lowick, S.E., Preusser, F., Anselmetti, F.S., Drescher-Schneider, R., Graf, H.R., Heller,
572 F., Horstmeyer, H., Kemna, H.A., Nowaczyk, N.R., Züger, and Furrer, H.: Evolution of an
573 overdeepened trough in the northern Alpine Foreland at Niederweningen, Switzerland. *Quat.*
574 *Sci. Rev.*, 34, 127-145, <https://doi.org/10.1016/j.quascirev.2011.12.015>, 2012.
- 575 Delaney, I., Anderson, L., and Herman, F.: Modelling the spatially distributed nature of subglacial
576 sediment transport and erosion. *Earth Surf. Dyn.*, 11, 663-680, <https://doi.org/10.5194/esuf-11-663-2023>, 2023.
- 578 Dieleman, C., Christl, M., Vockenhuber, C., Guatschi, P., Graf, H.R., and Akçar, N.: Age of the Most
579 Extensive Glaciation in the Alps. *Geosciences*, 12, 39,
580 <https://doi.org/10.3390/geosciences12010039>, 2022.
- 581 Dietrich, P., Griffis, N. P., Le Heron, D. P., Montañez, I. P., Kettler, C., Robin, C., and Guillocheau, F.:
582 Fjord network in Namibia: A snapshot into the dynamics of the late Paleozoic glaciation.
583 *Geology*, 49, 1521-1526, <https://doi.org/10.1130/G49067.1>, 2021.
- 584 Douillet, G., Ghienne, J. F., Géraud, Y., Abueladas, A., Diraison, M., and Al-Zoubi, A.: Late Ordovician
585 tunnel valleys in southern Jordan. *Geol. Soc. London Spec. Publ.*, 368, 275-292,
586 <https://doi.org/10.1144/sp368.4>, 2012.
- 587 Dürst Stucki, M., Reber, R., and Schlunegger, F.: Subglacial tunnel valleys in the Alpine foreland: An
588 example from Bern, Switzerland. *Swiss J. Geosci.*, 103, 363-374.
589 <https://doi.org/10.1007/s00015-010-0042-0>, 2010.
- 590 Dürst-Stucki, M., and Schlunegger, F.: Identification of erosional mechanisms during past glaciations
591 based on a bedrock surface model of the central European Alps. *Earth Planet. Sci. Lett.*, 384,
592 57-70. <https://doi.org/10.1016/j.epsl.2013.10.009>, 2013.
- 593 Egholm, D.L., Nielsen, S., Pedersen, V., and Lesemann, J.: Glacial effects limiting mountain height.
594 *Nature*, 460, 884-887, <https://doi.org/10.1038/nature08264>, 2009.
- 595 Fischer, U., and Häberli, W.: Overdeepenings in glacial systems: Processes and uncertainties. *Eos*, 93,
596 35, 341-341, <https://doi.org/10.1029/2012EO350010>, 2012.
- 597 Garefalakis, P., and Schlunegger, F.: Tectonic processes, variations in sediment flux, and eustatic sea
598 level recorded by the 20 Myr old Burdigalian transgression in the Swiss Molasse basin. *Solid*
599 *Earth*, 10, 2045-2972, <https://doi.org/10.5194/se-10.2045-2019>, 2019.
- 600 Gees: Spühlbohrung Bern B1. Wasser und Energiewirtschaft des Kantons Bern, 1974.
- 601 Gegg, L., Deplazes, G., Keller, L., Madritsch, H., Spillmann, T., Anselmetti, F. S., and Büchi, M.W.:
602 3D morphology of a glacially overdeepened trough controlled by underlying bedrock geology.
603 *Geomorphology*, 394, 107950. <https://doi.org/10.1016/j.geomorph.2021.107950>, 2021.
- 604 Gegg, L., and Preusser, F.: Comparison of overdeepened structures in formerly glaciated areas of the
605 northern Alpine foreland and northern central Europa. *E&G Quat. Sci. J.*, 72, 23-36.
606 <https://doi.org/10.5194/egqsj-72-23-2023>, 2023.



- 607 Geotest: Grundlagen für Schutz und Bewirtschaftung der Grundwasser des Kantons Bern.
608 Hydrogeologie Gürbetal und Stockental. Wasser- und Energiewirtschaftsamt des Kantons Bern
609 WEA, 123 pp, 1995.
- 610 Gerber, E.: Geologische Karte von Bern und Umgebung 1:25'000. Kümmerli und Frei, Bern, 1927.
- 611 Geyh, M.A., and Müller, H.: Palynological and geochronological study of the
612 Holsteinian/Hoxnian/Landos interglacial, in: The Climate of Past Interglacials, edited by:
613 Sirocko, F., Elsevier, Boston, MA, 387-396, 2007.
- 614 Gislser, C., Labhart, T., Spillmann, P., Herwegh, M., Della Valla, G., Trüssel, M., and Wiederkehr, M.:
615 Erläuterungen. Geologischer Atlas der Schweiz 1:25'000, 1210 Innertkirchen, Schweiz. Geol.
616 Komm., 2020.
- 617 Gupta, S., Collier, J.S., Palmer-Felgate, A., and Potter, G.: Catastrophic flooding origin of shelf valley
618 systems in the English Channel. *Nature*, 448, 342-345. <https://doi.org/10.1038/nature06018>,
619 2007.
- 620 Gupta, S., Collier, J. S., Garcia-Moreno, D., Oggioni, F., Trentesaux, A., Vanneste, K., De Batist, M.,
621 Camelbeeck, T., Potter, G., Van Vliet-Lanoë, B., and Arthur, J. C. R.: Two-stage opening of
622 the Dover Strait and the origin of island Britain. *Nat. Comm.*, 8, 15101.
623 <https://doi.org/10.1038/ncomms15101>, 2017.
- 624 Häberli, W., Linsbauer, A., Cochachin, A., Salazar, C., and Fischer, U.H.: On the morphological
625 characteristics of overdeepenings in high-mountain glacier beds. *Earth Surf. Proc. Landf.*, 41,
626 1980–1990, <https://doi.org/10.1002/esp.396>, 2016.
- 627 Hantke, R., and Scheidegger, A. E.: Zur Genese der Aareschlucht (Berner Oberland, Schweiz). *Geogr.*
628 *Helv.*, 48, 120–124. <https://doi.org/10.5194/gh-48-120-1993>, 1993.
- 629 Harvey, A. H.: Properties of Ice and Supercooled Water, in: CRC Handbook of Chemistry and Physics
630 (97th ed.), edited by Haynes, W. Lide, D. R. and Bruno, T., Boca Raton, FL: CRC Press., 2017.
- 631 Häuselmann, P., Granger, D.E., Jeannin, P.-Y., and Lauritzen, S.-E.: Abrupt glacial valley incision at
632 0.8 Ma dated from cave deposits in Switzerland. *Geology*, 35, 143-146,
633 <https://doi.org/10.1130/G23094A>, 2007.
- 634 Herman, F., and Braun, J.: Evolution of the glacial landscape of the Southern Alps of New Zealand:
635 insights from a glacial erosion model. *J. Geophys. Res.* 113, F02009,
636 <https://doi.org/10.1029/2007JF000807>, 2008.
- 637 Herman, F., Beaud, F., Champagnac, J.-D., Lemiux, J.-M., and Sternai, P.: Glacial hydrology and
638 erosion patterns: a mechanism for carving glacial valleys. *Earth Planet. Sci. Lett.* 310, 498–508,
639 <https://doi.org/10.1016/j.epsl.2011.08.022>, 2011.
- 640 Herman, F., Beyssac, O., Brughelli, M., Lane, S.N., Leprince, S., Adatte, T., Lin, J.Y.Y., Avouac, J.-
641 P., and Cox, S.C.: Erosion by an Alpine glacier. *Science*, 350, 193-195.
642 <https://doi.org/10.1126/science.aab2386>.



- 643 Hinderer, M. Late Quaternary denudation of the Alps, valley and lake fillings and modern river loads.
644 *Geodinamica Acta*, 14, 231-263, <https://doi.org/10.1080/09853111.2001.11432446>, 2001.
- 645 Hooke, R.L., and Pohjola, V.A.: Hydrology of a segment of a glacier situated in an overdeepening,
646 Storglaciären, Sweden. *J. Glaciol.*, 40, 140-148.
- 647 Isenschmid, C.: Die Grenze Untere Süsswassermolasse/Obere Meeremolasse als Schlüssel zur Tektonik
648 in der Region Bern. *Mitt. Natf. Ges. Bern*, 76, 108–133, 2019.
- 649 Ivy-Ochs, S., Kerschner, H., Reuther, A., Preusser, F., Heine, K., Maisch, M., Kubik, P. W., and
650 Schlüchter, C.: Chronology of the last glacial cycle in the European Alps. *J. Quat. Sci.*, 23, 559–
651 573. <https://doi.org/10.1002/jqs.1202>, 2008.
- 652 Jansen, J.D., Codilean, A.T., Stroeven, A.P., Fabel, D., Hättestrand, C., Kleman, J., Harbor, J.M.,
653 Heyman, J., Kubik, P.W., and Xu, S.: Inner gorges cut by subglacial meltwater during
654 Fennoscandian ice sheet decay. *Nat. Comm.*, 5, 3815, <https://doi.org/10.1038/ncomms4815>,
655 2014.
- 656 Jørgensen, F., and Peter B.E. Sandersen, P.B.E.: Buried and open tunnel valleys in Denmark—erosion
657 beneath multiple ice sheets. *Quat. Sci. Rev.*, 25, 1339–1363,
658 <https://doi.org/10.1016/j.quascirev.2005.11.006>, 2006.
- 659 Jordan, P.: Analysis of overdeepened valleys using the digital elevation model of the bedrock surface
660 of northern Switzerland. *Swiss J. Geosci.*, 103, 375–384, <https://doi.org/10.1007/s00015-010-0043-z>, 2010.
- 662 Kamleitner, S., Ivy-Ochs, S., Manatschal, L., Akçar, N., Christl, M., Vockenhuber, C., Hajdas, I., Synal,
663 H.-A.: Last glacial maximum glacier fluctuations on the northern Alpine foreland:
664 Geomorphological and chronological reconstructions from the Rhine and Reuss glacier
665 systems. *Geomorphology*, 423, 108548. <https://doi.org/10.1016/j.geomorph.2022.108548>,
666 2023a.
- 667 Kamleitner, S., Ivy-Ochs, S., Salcher, B., and Reitner, J.M.: Reconstructing basal ice flow patterns of
668 the Last Maximum Rhine glacier (northern Alpine foreland) based on streamlined subglacial
669 landforms. *Earth Surf. Proc. Landforms*, 49, 746-769, <https://doi.org/10.1002/esp.5733>, 2023b.
- 670 Kehew, A.E., Piotrowski, J.A., and Jørgensen, F.: Tunnel valleys: concepts and controversies – a
671 review. *Earth-Sci. Rev.* 113, 33–58, <https://doi.org/10.1016/j.earscirev.2012.02.002>, 2012.
- 672 Keller, B., Bläsi, H.-R., Platt, N., Mozley, P., and Matter, A.: Sedimentäre Architektur der distalen
673 Unteren Süsswassermolasse und ihre Beziehung zur Diagenese und den petrophysikalischen
674 Eigenschaften am Beispiel der Bohrungen Langenthal. NTB 90-41, *Landeshydrologie und –*
675 *geologie, Geologische Berichte*, 13, 100 pp, 1990.
- 676 Keller, O. and Krayss, E.: Mittel- und spätpleistozäne Stratigraphie und Morphogenese in
677 Schlüsselregionen der Nordschweiz. *E&G Quat. Sci. J.*, 59, 88–119, 2010.



- 678 Kellerhals, P., and Häfeli, C.: Brunnenbohrung Münsingen. Geologische Dokumentation des Kantons
679 Bern, WEA-Geologie, Beilage Nr. 2, 7 pp, 1984.
- 680 Kissling, E., Schwendener, H.: The Quaternary sedimentary fill of some Alpine valleys by gravity
681 modeling. *Eclogae Geol. Helv.*, 83, 311–321, 1990.
- 682 Koutsodendris, A., Pross, J., Müller, U. C., Brauer, A., Fletcher, W. J., Kühl, N., Kirilova, E., Verhagen,
683 F. T., Lücke, A., and Lotter, A. F.: A short-term climate oscillation during the Holsteinian
684 interglacial (MIS 11c): An analogy to the 8.2ka climatic event?, *Global Planet. Chang.*, 92–93,
685 224–235, <https://doi.org/10.1016/j.gloplacha.2012.05.011>, 2012.
- 686 Krohn, C. F., Larsen, N. K., Kronborg, C., Nielsen, O. B., and Knudsen, K.: L. Litho- and
687 chronostratigraphy of the Late Weichselian in Vendyssel, northern Denmark, with special
688 emphasis on tunnel-valley infill in relation to a receding ice margin. *Boreas*, 38, 811–833,
689 <https://doi.org/10.1111/j.1502-3885.2009.00104.x>, 2009.
- 690 Kühni, A., and Pfiffner, O.A.: The relief of the Swiss Alps and adjacent areas and its relation to lithology
691 and structure: topographic analysis from a 250-m DEM. *Geomorphology*, 41, 285–307,
692 [https://doi.org/10.1016/S0169-555X\(01\)00060-5](https://doi.org/10.1016/S0169-555X(01)00060-5), 2001.
- 693 Liebl, M., Robl, J., Hergarten, S., Egholm, D.L., and Stüwe, K.: Modeling large-scale landform
694 evolution with a stream power law for glacial erosion (OpenLEM v37): benchmarking
695 experiments against a more process-based description of ice flow (iSOSIA v3.4.3). *Geosci.
696 Model Dev.*, 16, 1315–1343, <https://doi.org/10.5194/gmd-16-1315-2023>, 2023.
- 697 Lisiecki, L.E., and Raymo, M.E.: A Pliocene-Pleistocene stack of 57 globally distributed benthic $d^{18}O$
698 records. *Paleoceanography*, 20, PA1003, <https://doi.org/10.1029/2004PA001071>, 2005.
- 699 Lloyd, C., Clark, C.D., and Swift, D.A.: The effect of valley confluence and bedrock geology upon the
700 location and depth of glacial overdeepenings. *Geogr. Ann.: Series A, Phys. Geogr.*,
701 <https://doi.org/10.1080/04353676.2023.2217047>, 2023.
- 702 Lohrberg, A., Schneider von Deimling, J., Grob, H., Lenz, K.-F., and Krastel, S.: Tunnel valleys in the
703 southeastern North Sea: More data, more complexity. *E&G Quat. Sci. J.*, 71, 267–274,
704 <https://doi.org/10.5194/egqsj-71-267-2022>, 2022.
- 705 Moreau, J., Huuse, M., Janszen, A., van der Vegt, P., Gibbard, P. L., and Moscriello, A.: The
706 glaciogenic unconformity of the southern North Sea. *Geol. Soc. London Spec. Publ.*, 368, 99.
707 <https://doi.org/10.1144/SP368.5>, 2012.
- 708 Montgomery, D. R., and Korup, O.: Preservation of inner gorges through repeated Alpine glaciations.
709 *Nat. Geosci.*, 4, 62–67. <https://doi.org/10.1038/Ngeo1030>, 2011.
- 710 Nagy, D.: The gravitational attraction of a right rectangular prism. *Geophysicis*, 31, 362–271, 1996.
- 711 Nishiyama, R., Ariga, A., Ariga, T., Lechmann, A., Mair, D., Pistillo, C., Scampoli, P., Valla, P.G.,
712 Vladymyrov, M., Ereditato, A., and Schlunegger, F.: Bedrock sculpting under an active alpine



- 713 glacier revealed from cosmic-ray muon radiography. *Sci. Rep.*, 9, 6970,
714 <https://doi.org/10.1038/s41598-019-43527-6>, 2019.
- 715 Nørgaard, J., Jansen, J.D., Neuhuber, S., Ruzkiczay-Rüdiger, Z., Knudsen, M.F.: P-PINI: A
716 cosmogenic nuclide burial dating method for landscapes undergoing non-steady erosion. *Quat.*
717 *Geochron.*, 74, 101420, <https://doi.org/10.1016/j.quageo.2022.101420>, 2023.
- 718 Ottesen, D., Stewart, M., Brönnner, M., and Batchelor, C. L.: Tunnel valleys of the central and northern
719 North Sea (56°N to 62°N): Distribution and characteristics, *Mar. Geol.*, 425, 106199,
720 <https://doi.org/10.1016/j.margeo.2020.106199>, 2020.
- 721 Patton, H., Swift, D. A., Clark, C. D., Livingstone, S. J., and Cook, S. J.: Distribution and characteristics
722 of overdeepenings beneath the Greenland and Antarctic ice sheets: Implications for
723 overdeepening origin and evolution. *Quat. Sci. Rev.*, 148, 128–145,
724 <https://doi.org/10.1016/j.quascirev.2016.07.012>, 2016.
- 725 Pedersen, V.K., and Egholm, D.L.: Glaciations in response to climate variations preconditioned by
726 evolving topography. *Nature*, 493, 206–201, <https://doi.org/10.1038/nature11786>, 2013.
- 727 Perrouy, S., Moussirou, B., Martinod, J., Banvalot, S., Carretier, S., Gabalda, G., Monod, B., Hérail,
728 G., Regard, V., and Remy, D.: Geometry of two glacial valleys in the northern Pyrenees
729 estimated using gravity data, *Comptes Rendus Geosci.*, 347, 13–23,
730 <https://doi.org/10.1016/j.crte.2015.01.002>, 2015.
- 731 Pfander, J., Schlunegger, F., Serra, E., Gribenski, N., Garefalakis, P., and Akçar, N.: Glaciofluvial
732 sequences recording the Birrfeld Glaciation (MSS 5d-2) in the Bern area, Swiss Plateau. *Swiss*
733 *J. Geosci.*, 115, 12, <https://doi.org/10.1186/s00015-022-00414-z>, 2022.
- 734 Piotrowski, J.A.: Subglacial hydrology in north-western Germany during the last glaciation:
735 Groundwater flow, tunnel valleys and hydrological cycles. *Quat. Sci. Rev.*, 16, 169–185,
736 [https://doi.org/10.1016/S0277-3791\(96\)00046-7](https://doi.org/10.1016/S0277-3791(96)00046-7), 1997.
- 737 Preusser, F., and Schlüchter, C. Dates from an important early Late Pleistocene ice advance in the Aare
738 valley, Switzerland. *Eclogae Geol. Helv.*, 97, 245–253. <https://doi.org/10.1007/s00015-004-1119-4>, 2004.
- 740 Preusser, F., Drescher-Schneider, R., Fiebig, M., and Schlüchter, C.: Re-interpretation of the Meikirch
741 pollen record, Swiss Alpine Foreland, and implications for Middle Pleistocene
742 chronostratigraphy. *J. Quat. Sci.*, 20., 607–620, <https://doi.org/10.1002/jqs.930>, 2005.
- 743 Preusser, F., Reitner, J. M., and Schlüchter, C.: Distribution, geometry, age and origin of overdeepened
744 valleys and basins in the Alps and their foreland. *Swiss J. Geosci.*, 103, 407–426.
745 <https://doi.org/10.1007/s00015-010-0044-y>, 2010.
- 746 Preusser, F., Graf, H. R., Keller, O., Krayss, E., and Schlüchter, C.: Quaternary glaciation history of
747 Northern Switzerland. *E&G Quat. Sci. J.*, 60, 282–305, <https://doi.org/10.3285/eg.60.2-3.06>,
748 2011.



- 749 Preusser, F., Büschelberger, M., Kemma, H.A., Miodic, J., Müller, D. and May, J.-H.: Exploring
750 possible links between Quaternary aggradation in the Upper Rhine Graben and the glaciation
751 history of northern Switzerland. *Int. J. Earth Sci.*, 110, 1827-1846,
752 <https://doi.org/10.1007/s00531-021-02043-7>, 2021.
- 753 Railsback, L.B., Gibbard, P.L., Head, M.J., Voarintsoa, N.R.G., and Toucanne, S.: An optimized
754 scheme of lettered marine isotope substages for the last 1.0 million years, and the
755 climatostratigraphic nature of isotope stages and substages. *Quat. Sci. Rev.*, 111, 94-106,
756 [10.1016/j.quascirev.2015.01.012](https://doi.org/10.1016/j.quascirev.2015.01.012), 2015.
- 757 Reber, R., Akçar, N., Ivy-Ochs, S., Tikhomirov, D., Burkhalter, R., Zahno, C., Lüthold, A., Kubik,
758 P.W., Vockenhuber, C., and Schlüchter, C.: Timing of retreat of the Reuss Glacier
759 (Switzerland) at the end of the Last Glacial Maximum. *Swiss J. Geosci.*, 107, 293-307,
760 <https://doi.org/10.1007/s00015-014-0169-5>, 2014.
- 761 Reber, R., and Schlunegger, F.: Unravelling the moisture sources of the Alpine glaciers using tunnel
762 valleys as constraints. *Terra Nova*, 28, 202–211, <https://doi.org/10.1111/ter.12211>, 2016.
- 763 Reitner, J.M., Gruber, W., Römer, A., and Morawetz, R.: Alpine overdeepenings and paleo-ice flow
764 changes: an integrated geophysical-sedimentological case study from Tyrol (Austria). *Swiss J.*
765 *Geosci.*, 103, 385-405, <https://doi.org/10.1007/s00015-010-0046-9>, 2010.
- 766 Roger, S., Féraud, G., de Beaulieu, J.-L., Thouveny, N., Coulon, Ch., Choucem., J.J., Andrieu, V. and
767 Williams, T.: $^{40}\text{Ar}/^{39}\text{Ar}$ dating on tephra of the Velay maars (France): implications for the
768 Late Pleistocene proxy-climatic record. *Earth Planet Sci. Lett.*, 170: 287–299, 1999.
- 769 Ross, N., Siegert, M.J., Woodward, J., Smith, A.M., Corr, H.F.J., Bentley, M.J., Hindsmarsh, R.C.A.,
770 King, E.C., and Rivera, A.: Holocene stability of the Amundsen-Weddell ice divide, West
771 Antarctica. *Geology*, 39, 935-938, <https://doi.org/10.1130/G31920>, 2011.
- 772 Rosselli, A., and Raymond, O. : Modélisation gravimétrique 2.5D et cartes des isohypses au 1:100'000
773 du substratum rocheux de la Vallée du Rhône entre Villeneuve et Brig (Suisse). *Eclogae Geol.*
774 *Helv.*, 96, 399–423, 2003.
- 775 Schaller, S., Büchi, M.W., Schuster, B., and Anselmetti, F.: Drilling into a deep buried valley (ICDP
776 DOVE): a 252 m long sediment succession from a glacial overdeepening in northwestern
777 Switzerland. *Sci. Drill.*, 32, 27-42, <https://doi.org/10.5194/sd-32-27-2023>, 2023.
- 778 Schläfli, P., Gobet, E., van Leeuwen, J.F.N., Vescovi, E., Schwenk, M.A., Bandou, D., Douillet, G.A.,
779 Schlunegger, F., and Tinner, W.: Palynological investigations reveal Eemian interglacial
780 vegetation dynamics at Spiezberg, Bernese Alps, Switzerland. *Quat. Sci. Rev.*, 263, 106975,
781 <https://doi.org/10.1016/j.quascirev.2021.106975>, 2021.
- 782 Schlüchter, C.: The deglaciation of the Swiss-Alps: a paleoclimatic event with chronological problems.
783 *Bull. l'Association française pour l'étude du Quat.*, 25 , 141-145, 1988.



- 784 Schlüchter, C.: Thalgot: ein umfassendes eiszeit stratigraphisches Referenzprofil im nördlichen
785 Alpenvorland. *Eclogae geol. Helv.*, 82, 277-284, 1989.
- 786 Schlüchter, C. The Swiss glacial record – a schematic summary. *Develop. Quat. Sci.*, 2, 413-418,
787 [https://doi.org/10.1016/S1571-0866\(04\)80092-7](https://doi.org/10.1016/S1571-0866(04)80092-7), 2004.
- 788 Schlunegger, F., and Garefalakis, P.: Einführung in die Sedimentologie, Schweizerbart, Stuttgart,
789 www.schweizerbart.de/9783510655397, 2023.
- 790 Schwenk, M., Schläfli, P., Bandou, D., Gribenski, N., Douillet, G., and Schlunegger, F.: From glacial
791 erosion to basin overfill: A 240 m-thick overdeepening-fill sequence in Bern. Switzerland. *Sci.*
792 *Drill.*, 30, 17–42, <https://doi.org/10.5194/sd-30-17-2022>, 2022a.
- 793 Schwenk, M. A., Stutenbecker, L., Schläfli, P., Bandou, D., and Schlunegger, F.: Two glaciers and one
794 sedimentary sink: The competing role of the Aare and the Valais glaciers in filling an
795 overdeepened trough inferred from provenance analysis. *E&G Quat. Sci. J.*, 71, 163–190,
796 <https://doi.org/10.5194/egqsj-71-163-2022>, 2022b.
- 797 Steinemann, O., Ivy-Ochs, S., Hippe, K., Christl, M., Naghipour, N., and Synal, H.-A.: Glacial erosion
798 by the Trift glacier (Switzerland): Deciphering the development of riegels, rock basins and
799 gorges. *Geomorphology*, 375, 107533, <https://doi.org/10.1016/j.geomorph.2020.107533>, 2021.
- 800 Stewart, M.A., and Lonergan, L.: Seven glacial cycles in the middle-late Pleistocene of northwest
801 Europe: geomorphic evidence from buried tunnel valleys. *Geology* 39, 283-286,
802 <https://doi.org/10.1130/G31631.1>, 2011.
- 803 Stewart, M.A., Lonergan, L. and Hampson, G.: 3D seismic analysis of buried tunnel valleys in the
804 central North Sea: tunnel valley-fill sedimentary architecture, in: *Glaciogenic Reservoirs and*
805 *Hydrocarbon Systems*, edited by: Huuse, M., Redfern, J., Le Heron, D.P., Dixon, R.J., and
806 Moscardiello, A.. *Geol. Soc. London Spec. Publ.*, 368, 173-183,
807 <http://dx.doi.org/10.1144/SP368.9>, 2013.
- 808 Valla, P.G., van der Beek, P.A., and Carcaillet, J.: Dating bedrock gorge incision in the French Western
809 Alps (Ecrins-Pelvoux massif) using cosmogenic ¹⁰Be. *Terra Nova*, 22, 18-25,
810 <https://doi.org/10.1111/j.1365-1321.2009.00911.x>, 2010.
- 811 Valla, P., Shuster, D.L., and van der Beek, P.A.: Significant increase in relief of the European Alps
812 during mid-Pleistocene glaciations. *Nat. Geosci.*, 4, 688-692,
813 <https://doi.org/10.1038/ngeo1242>, 2011.
- 814 Welten, M.: Pollenanalytische Untersuchungen im jüngeren Quartär des nördlichen Alpenvorlandes der
815 Schweiz. *Beitr. Geol. Karte Schweiz*, 156, 174 pp., 1982.
- 816 Welten, M.: Neue pollenanalytische Ergebnisse über das jüngere Quartär des nördlichen
817 Alpenvorlandes der Schweiz (Mittel-und Jungpleistozän). *Beitr. Geol. Karte Schweiz*, 162, 9-
818 40, 1988.



- 819 Wright, H. E.: Tunnel valleys, glacial surges, and subglacial hydrology of the Superior Lobe, 340
820 Minnesota. Mem. Geol. Soc. Amer., 136, 251-276, <https://doi.org/10.1130/MEM136-p251>,
821 1973.
- 822 Zwahlen, P., Tinner, W. and Vescovi, E.: Ein neues EEM-zeitliches Umweltarchiv am Spiezberg
823 (Schweizer Alpen) im Kontext der mittel- und spätpleistozänen Landschaftsentwicklung. Mitt.
824 Naturf. Ges. Bern 78, 92–121, 2021.